MODEL-BASED CONTROL OF AN RCCI ENGINE

By

Akshat Abhay Raut

A THESIS

Submitted in partial fulfillment of the requirements for the degree of

MASTER OF SCIENCE

In Mechanical Engineering

MICHIGAN TECHNOLOGICAL UNIVERSITY

2017

This thesis has been approved in partial fulfillment of the requirements for the Degree of MASTER OF SCIENCE in Mechanical Engineering.

Department of Mechanical Engineering - Engineering Mechanics

Thesis Advisor: *Dr. Mahdi Shahbakhti*

Committee Member: *Dr. Scott Miers*

Committee Member: *Dr. Seyyedmohsen Azizi*

Department Chair: *Dr. William W. Predebon*

Dedication

To my parents Vidula and Abhay and my brother Archit

Contents

List of Figures

List of Tables

Acknowledgments

I would like to thank my family for being a constant source of support.

I would like to thank Dr Shahbakhti for giving me the opportunity to work under him and for his patience and constant words of encouragement while guiding me in my research.

I would like my extend my gratitude to Dr Miers and Dr Azizi for taking time out of their schedule and agreeing to be part of my committee.

A very special thank you goes out to Jayant, Kaushik, Hamit, Nitin, Mehran and all other members of the EML group whose prior work set the foundation for my research.

I would like to extend my gratitude to Karan and Behrouz for being wonderful lab partners and for helping me out with my experiments.

I would also like to thank Dr Ali Borhan from Cummins Inc. for his valuable inputs on MPC design and implementation.

Special thanks to Paul and Joel and everyone at APS labs.

List of Abbreviations

AFR	Air Fuel Ratio
BDC	Bottom Dead Centre
BEV	Battery Electric Vehicle
CAD aTDC	Crank Angle Degrees after Top Dead Centre
CAD bTDC	Crank Angle Degrees before Top Dead Centre
CDC	Conventional Diesel Combustion
CFD	Computational Fluid Dynamics
CN	Cetane Number
CO	Carbon Monoxide
COM	Control Oriented Model
COV	Coefficient of Variation
DARE	Discrete-time Algebraic Riccati Equation
DI	Direct Injection
EVC	Exhaust Valve Closing
EVO	Exhuast Valve Opening
FAR	Fuel Air Ratio
FCV	Fuel Cell Vehicle
FPGA	Field Programmable Gate Array

FQ	Total Fuel Quantity
GDI	Gasoline Direct Injection
GHG	Green House Gases
HCCI	Homogeneous Charge Compression Ignition
HP	Horse Power
HRR	Heat Release Rate
ICE	Internal Combustion Engines
ID	Ignition Delay
IMEP	Indicated Mean Effective Pressure
IVC	Intake Valve Closing
IVO	Intake Valve Opening
LHV	Lower Heating Value
LTC	Low Temperature Combustion
MABX	Micro Auto Box
MIMO	Multi Input Multi Output
MKIM	Modified Knock Integral Model
mpg	miles per gallon
MVM	Mean Value Model
PCCI	Premixed Charge Compression Ignition
PCI	Premixed Compression Ignition
PFI	Port Fuel Injection

PHEV	Plug-in Hybrid Electric Vehicle
PM	Particulate Matter
PR	Premixed Ratio
SCR	Selective Catalytic Reduction
SISO	Single Input Single Output
SOC	Start of Combustion
SOI	Start of Injection
TDC	Top Dead Centre
UHC	Unburnt Hydrocarbons

Symbols

c_v	Specific heat at constant volume (kJ/kg.K)
LHV	Lower heating value (MJ/kg)
m_{air}	mass of air (g/s)
m_{fuel}	total mass of fuel (mg/cycle)
N	Engine speed (RPM)
n_c	Compression polytopic coefficient (-)
n_e	Expansion polytropic coefficient (-)
P_{in}	Intake pressure (kPa)
P_{ivc}	Pressure at intake valve closing (kPa)

r_c	Compression ratio (-)
S	Sensitivty (-)
S_{ig}	Spontaneous ignition front speed (m/s)
$T_{exhaust}$	Exhaust temperature (K)
T_{in}	Intake Temperature (K)
T_{ivc}	Temperature at intake valve closing (K)
T_{rg}	Residual gas temperature (K)
U_x	Uncertainity in measured parameters
U_y	Uncertainity in derived parameters
V	volume (m^3)
x	Fuel film fraction (-)
X	State vector
x_b	Mass fraction burnt (-)
$\Delta\phi$	Gradient of equivalence ratio (-)
ΔT	Temperature rise (K)
ΔT_m	Time delay (sec)
$\dot{m}_f$	Total fuel entering the cylinder per cycle (mg/cycle)
$\dot{m}_{ff}$	Fuel entering the cylinder from the fuel film (mg/cycle)
$\dot{m}_{fi}$	Fuel injected into the intake port per cycle (mg/cycle)
$\dot{m}_{fv}$	Fuel entering the cylinder in vapor phase (mg/cycle)
γ	Ratio of specific heats (-)

$\hat{X}$	Estimated state vector
Λ	Ratio of actual AFR to stoichiometric AFR (-)
ϕ	Equivalence ratio (-)
τ	Ignition delay (sec)
τ_f	Time constant of fuel film (sec)
τ_m	Time constant of lambda sensor (sec)
θ	Crank angle (CAD)

Subscripts

aug	augmented
c	compression
d	burn duration
d	burn duration
DI	direct injection
dis	displaced
e	expansion
eoc	end of combustion
evc	exhaust valve closing
evo	exhaust valve opening
exh	exhaust
f	fuel
i	prediction step

in	intake
iso	iso-octane
ivc	Intake valve closing
ivo	intake valve closing
k	engine cycle
mix	mixture
nhep	n-heptane
PFI	port-fuel injection
rg	residual gas
soc	start of combustion
st	stoichiometric
t	total
tot	total

Abstract

Reactivity controlled compression ignition (RCCI) is a combustion strategy that offers high fuel conversion efficiency and near zero emissions of NOx and soot which can help in improving fuel economy in mobile and stationary internal combustion engine (ICE) applications and at the same time lower engine-out emissions. One of the main challenges associated with RCCI combustion is the difficulty in simultaneously controlling combustion phasing, engine load, and cyclic variability during transient engine operations.

This thesis focuses on developing model based controllers for cycle-to-cycle combustion phasing and load control during transient operations. A control oriented model (COM) is developed by using mean value models to predict start of combustion (SOC) and crank angle of 50% mass fraction burn (CA50). The COM is validated using transient data from an experimental RCCI engine. The validation results show that the COM is able to capture the experimental trends in CA50 and indicated mean effective pressure (IMEP). The COM is then used to develop a linear quadratic integral (LQI) controller and model predictive controllers (MPC). Premixed ratio (PR) and start of injection (SOI) are the control variables used to control CA50, while the total fuel quantity (FQ) is the engine variable used to control load. The selection between PR and SOI is done using a sensitivity based algorithm. Experimental validation results

for reference tracking using LQI and MPC show that the desired CA50 and IMEP can be attained in a single cycle during step-up and step-down transients and yield an average error of less than 1.6 crank angle degrees (CAD) in the CA50 and less than 35 kPa in the IMEP. This thesis presents the first study in the literature to design and implement LQI and MPC combustion controllers for RCCI engines.

Chapter 1

Introduction

The Annual Energy Outlook report of 2017 [1] predicts that by 2040 the major driving force in the transportation industry will still remain to be cars powered by internal combustion engines (ICEs) with less than 11% of the total light-duty vehicle sales coming from other sources such as plug-in hybrid vehicles (PHEV), battery electric vehicles (BEV) and hydrogen fuel cell vehicles (FCV) combined. The EPA regulations [2] for reduction in greenhouse gas (GHG) emissions for light duty vehicles require vehicles to achieve an average industry fleet-wide fuel economy of 54.5[1] miles per gallon (mpg) by 2025 in order to meet the CO2 emissions standards. To achieve this target a significant impetus is being given to technological research on advanced lean-burn combustion regimes, application of existing technologies such as cylinder

---

[1]Assuming reduction in CO2 is achieved exclusively through fuel economy improvements.

deactivation, turbocharging and downsizing, and higher market penetration of diesel engines [3]. Diesel engines provide higher thermal efficiency as compared to gasoline powered engines due to the use of higher compression ratios and unthrottled intake flow. However due to high peak temperatures achieved during combustion, emissions of NOx and particulate matter (PM) are higher [4] and require a costly aftertreatment system in diesel engines. Particulate traps are generally used for trapping PM emissions but they require frequent active or passive regeneration [5]. NOx emissions on the other hand can be tackled using selective catalytic reduction (SCRs) systems. SCRs use a reducing agent like ammonia or urea and these agents need to be continuously replenished for smooth operation of the SCR. As emission norms get stringent the cost of these aftertreatment technologies is on the rise leading to the search for alternative technologies.

1.1 Motivation towards LTC combustion

A potential strategy to tackle emissions and increase fuel economy of ICEs is through implementation of low temperature combustion (LTC) strategies. LTC combustion is based on the concept of lean burn to decrease the peak temperatures. Due to low in-cylinder temperature, the energy lost due to heat transfer is low [6] resulting in higher overall thermal efficiency. In addition, the intake air is unthrottled, thus removing throttling losses in ICEs. Forms of LTC combustion such as homogeneous charge

compression ignition (HCCI) and premixed charge compression ignition (PCCI) have been known to give near zero engine out emissions of NOx and PM [7] [8]. HCCI relies on auto-ignition of a homogeneous air-fuel mixture that has a very low equivalence ratio. The short combustion duration prevents operation at high loads due to high peak pressure rise rate. Various stratification techniques have been suggested to control knock [9]. However the lack of control over the combustion phasing and heat release rate is a major hurdle. HCCI and PCCI combustion strategies generally suffer from high carbon monoxide (CO) and unburnt hydrocarbon (UHC) emissions [10].

Kokjohn et. al. [11] explored the possibility of using dual-fuel operation in premixed compression ignition (PCI) engines as a method to control combustion phasing. Their experimental results showed that at low load conditions (6 bar IMEP) high amount (60%) of exhaust gas recirculation (EGR) was required to set combustion phasing to the optimal point when only diesel fuel was used. The amount of EGR used could be decreased significantly by using diesel blend with high amounts of gasoline (70 PRF). At high load conditions (11 bar IMEP) high amount of EGR (50%) and gasoline blends (80 PRF) were required for optimal combustion phasing. Even with the combustion phasing well after TDC, the pressure rise rate was rapid. They concluded that fuel reactivity is capable of combustion control but fuel stratification is required to control pressure rise rates. On further experimentation with in-cylinder blending of port fuel injected gasoline and direct injected diesel at high load conditions, low NOx and soot levels were observed with high indicated thermal efficiency (close to 50%).

CHEMKIN modeling results showed staged combustion with ignition location coinciding with the location having high concentration of diesel fuel. This extended the combustion duration; decreasing the heat release rate and pressure rise rate and allowing for controlled combustion at high loads. They termed this form of combustion as reactivity controlled compression ignition (RCCI).

RCCI combustion involves the use of two fuels of different reactivity. The low-reactivity fuel is injected into the intake port. This fuel is introduced in the cylinder as a homogeneous mixture with the intake air and EGR (if any). The high-reactivity fuel is then directly injected into the cylinder. The early injection of the high-reactivity fuel creates a reactivity gradient inside the cylinder, with pockets of charge rich in high-reactivity fuel igniting first. This is due to the high-reactivity reacting with low-temperature reactions, releasing enough energy to ignite the low-reactivity fuel [12]. This staged combustion helps to control the heat release rate. Figure 1.1 depicts the fuel injection setup in an RCCI engine.

Figure 1.2 shows a comparison between emissions of different LTC regimes and conventional diesel combustion (CDC). It can be seen that due to high local equivalence ratios and in cylinder temperature, CDC suffers from high soot formation and NOx emissions. LTC combustion typically occurs at a peak temperature of 1700 K [13] which prevents formation of NOx. Due to low local equivalence ratios, soot formation is negligible. However all LTC regimes suffer from high UHC and CO emissions, when
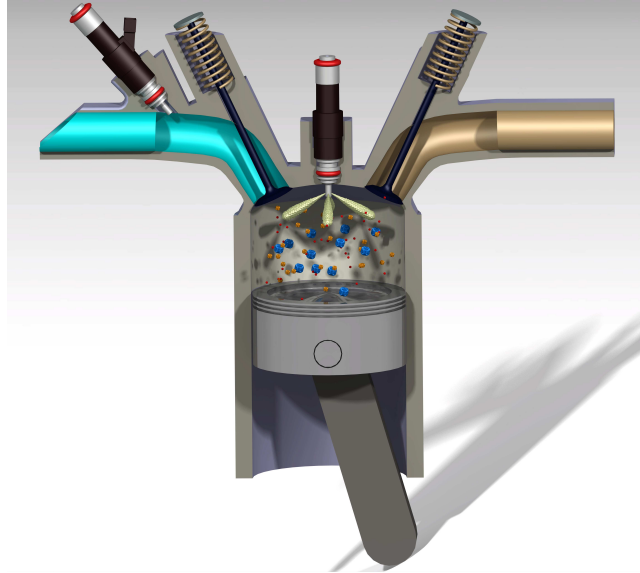
Figure 1.1: RCCI fuel injection setup. Low reactivity fuel is injected into the intake port while high reactivity fuel is directly injected into the cylinder.

LTC regimes are not fully optimized.
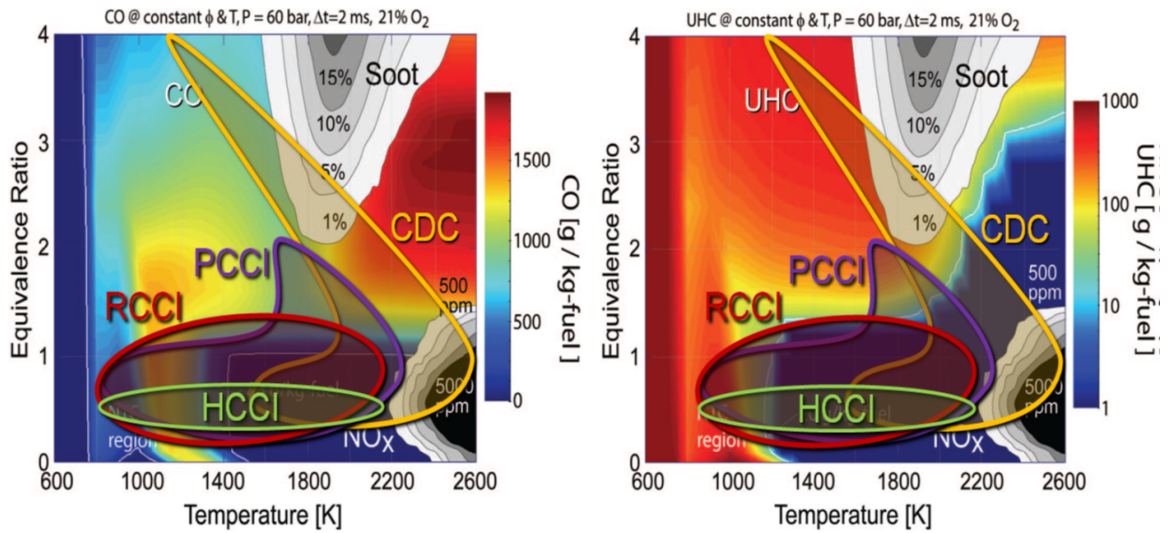
Figure 1.2: Contour plots showing NOx, CO, UHC and soot emissions with overlays of different combustion regimes [14]. CDC stands for conventional diesel combustion.

1.2   Prior studies in RCCI combustion

Extensive research regarding RCCI combustion modeling, performance and emissions has been conducted. Initial studies include comparison between RCCI and CDC combustion [15] and engine mapping studies [16]. Splitter et al studied the effects of varying injection timing [17] and using multiple injections [18]. Studies also include the use of alternative fuels such as natural gas [19] [20], methanol [21] and biodiesel [22]. Effect of using different piston bowl geometries [23] [24] and cetane number improvers [25] [26] have also been investigated. Figure 1.3 shows an overview of some of the prior RCCI studies.

Prior Studies in RCCI Engines: performance, fuel type, geometry

Exploiting Conventional Fuels	Injection Timing Effects	Cetane Number Improvers	Utilizing Alternative Fuels	Modified Piston Geometries
2011 • Kokjohn et al. – Comparison of RCCI for HD and LD engines at specific points. (Exp.& Modelling) **2013** • Curran et al. – Creation of RCCI engine map over wide speed and load • Splitter et al. – Obtained max. GTE of 59% at 6.5 bar IMEP and 1300 r/min **2015** • Kokjohn et al. – Optical investigation of combustion process to explain the role of ϕ, temp. and reactivity.	**2011** • Splitter et al. – Effects of DI timing with single and double injections of n-hep • Kokjohn et al. – Effect of SOI sweep to explore fuel reactivity stratification. **2012** • Wissink et al. – Effect of injecting both fuels by DI • Nieman et al. – Single and double injections of NG-diesel fuel in HD engine. **2014** • Benajes et al. – Investigate mixing and autoignition in RCCI **2015** • Wissink & Reitz – Direct dual fuel stratification	**2011** • Splitter et al. – Comparison of Gasoline-diesel, E85-diesel(duel fuel) with gasoline-gasoline+DTBP @ medium and high loads. **2013** • Dempsey et al. – Effects of CN improvers on fuel reactivity of gasoline, ethanol and methanol. **2015** • Wand et al. – Numerical investigation with various fuels- isobutanol-diesel, isobutanol-isobutanol+DTBP • Dempsey et al. – Single fuel Gasoline-Gasoline+ varying levels of 2-EHN	**2012** • Nieman et al. – Natural Gas – Diesel (HD Engine) **2013** • Soloiu et al. – n-butanol-biodiesel • Hanson et al. – E20-B20 **2014** • Li et al. – Parametric study of RCCI using Methanol-diesel • Brijesh et al. – Diesel-LPG **2015** • Zoldak et al. – Natural gas(NG) - Diesel • Zhou et al. – Investigation of knocking using biodiesel-methanol.	**2012** • Splitter et al. - Effects of Compression ratio and piston design in HD engine at varying loads **2013** • Dempsey et al. - Modified Piston with a shallow, flat piston bowl with no squish land **2014** • Lim and Reitz – Effectiveness of utilizing piston geometry for combustion control of RCCI **2015** • Lim and Reitz – Chamfered piston crown design for reducing UHC emissions

Figure 1.3: Overview of prior RCCI research in the areas ranging from fuel type to injection parameters and combustion chamber design [14] [15] [16] [17] [18] [19] [20] [21] [22] [23] [24] [25] [26] [27] [28] [29] [30] [31] [32] [33] [34] [35] [36] [37].

However, only a few studies are found for research in the field of closed loop control of RCCI combustion. Figure 1.4 shows an overview of prior studies in RCCI control.
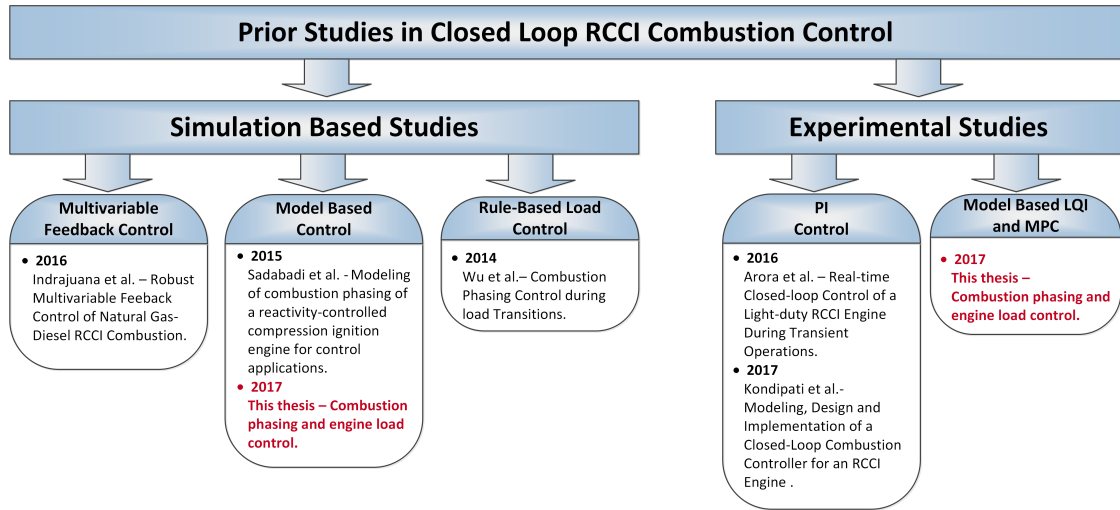
Figure 1.4: Overview of prior studies in RCCI combustion control [38] [39] [40] [41] [42] [43]

Wu et al. [39] used an experimentally validated GT-Power model to develop a control strategy to control combustion phasing during load step-up and step-down transients. They suggested using higher PR during step-down transients to offset the advance in CA50[1] caused by the slow intake pressure decrease. Similarly during step-up transients, the use of lower PR was recommended. Bekdemir et al. [40] developed a mean-value model for control of natural gas-diesel RCCI combustion. Indrajuana et al [41] developed a multivariable feedback control strategy for cycle-to-cycle control with simulation results for reference tracking and disturbance rejection cases. The Energy Mechatronics Lab (EML) team at Michigan Technological University has been doing

---

[1]Crank angle at 50% fuel mass fraction burnt.

7

research on RCCI combustion control for the past four years. Sadabadi [42] developed a physics based control oriented model (COM) to control combustion phasing. The model was validated using simulation data from an experimentally validated CFD combustion model. A linear quadratic integral controller was developed for CA50 control and validated using simulation data for reference traking and disturbance rejection cases. Kondipati [38] used experimental RCCI engine data to parametrize and validate a physics based dynamic model and implemented real-time PI control on an RCCI engine. Experimental validation results showed that the PI controller was able to track CA50 with a average error of 2 CAD. Arora [44] used a combination of feed-forward and feedback PI control to develop a controller for transient operation in light duty RCCI combustion applications. Arora et al. [43] proposed the use of a sensitivity map to determine whether PR or SOI be used as the control variable. This thesis builds upon the above mentioned works [38] [42] [43] to design and implement new model based control strategies for combustion phasing and load control during transient operation. To the best of the author's knowledge, *this thesis* presents the *first study* undertaken in literature to *design and implement model-based combustion control (i.e., LQI, MPC) strategies for RCCI engines.*

1.3 Research Goals

The goals of this thesis are as follows:

† To develop, and experimentally validate Mean Value Models (MVM) to predict start of combustion (SOC) and CA50.

† To develop a dynamic model to predict cycle-to-cycle combustion phasing and IMEP. The new dynamic model should include residual gas dynamics and fuel transport dynamics.

† To design and experimentally validate linear quadratic integral (LQI) controllers for RCCI combustion phasing control.

† To design and experimentally validate a multi input multi output (MIMO) model predictive controller (MPC) for combustion phasing and load control.

† To develop switched MPC controllers and implement a sensitivity based strategy for selecting between start of injection (SOI) and premixed ratio (PR) as the control variable. This new control strategy aims to control combustion for a large range of RCCI engine operation.

1.4   Organization of Thesis

Figure 1.5 gives an overview of this thesis. Chapter 2 discusses the experimental setup in detail. In Chapter 3, a dynamic model is developed to predict SOC and CA50. The model is parameterized using steady state experimental data and validated for engine transient operating conditions. In addition, new models to predict IMEP and
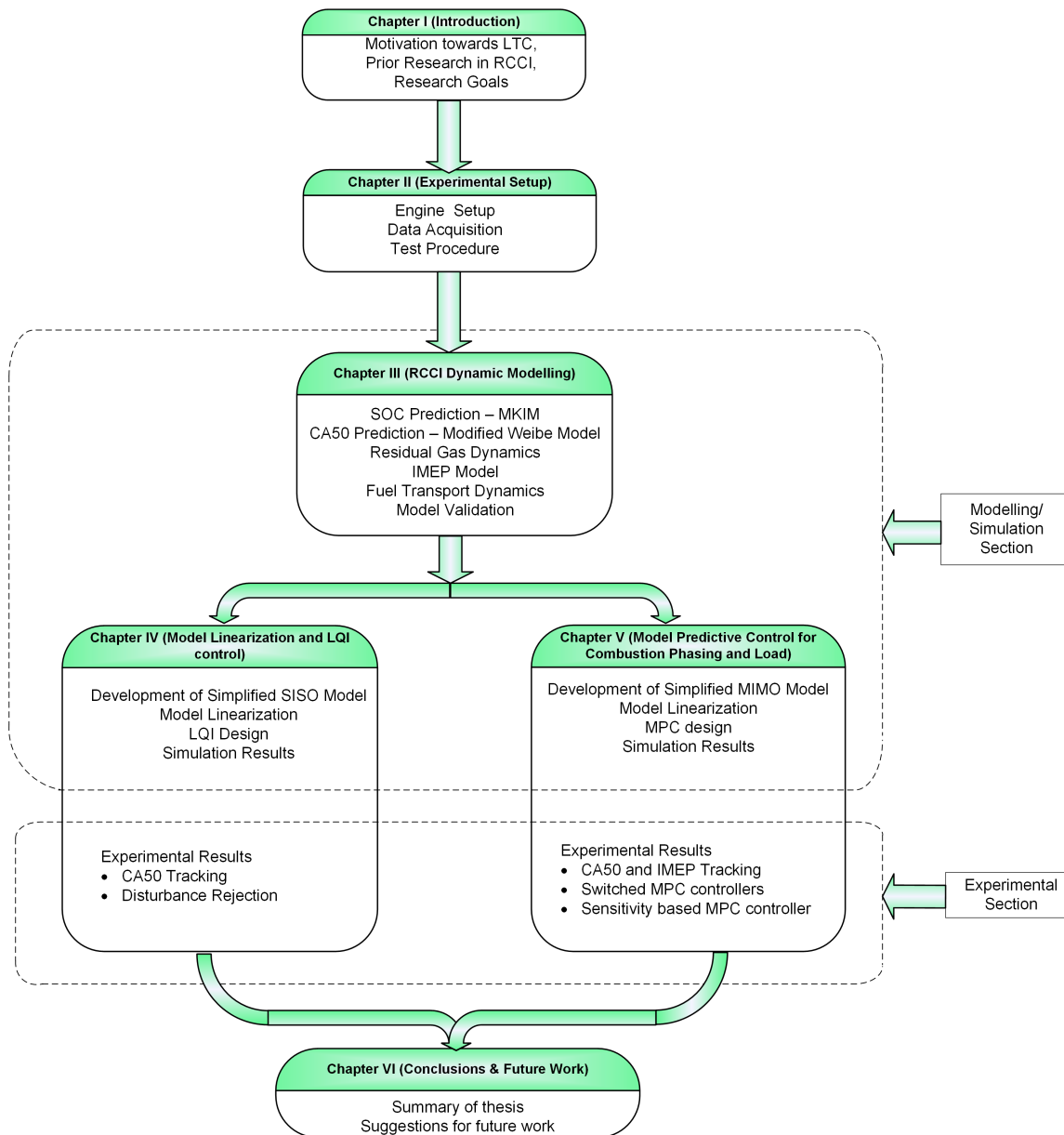
Figure 1.5: Thesis organization schematic

to account for fuel dynamics are developed. In Chapter 4, the dynamic model is

simplified and converted into state space form in order to design a Linear Quadratic

Integral controller to control combustion phasing. The controller is then evaluated on

the experimental setup. In Chapter 5, a MIMO model predictive controller is developed for combustion phasing and load control. Different MPC controllers including sensitivity based MPC are tested out on the experimental RCCI engine setup and discussed in detail. To conclude, a summary of the major contributions from this thesis is provided and recommendations for future work are described in Chapter 6.

Chapter 2

Experimental Setup

This chapter is divided into four parts. The first part introduces the engine test setup. The second part discusses the control and data acquisition systems. The third part explains the experimental test procedure and the fourth part describes the uncertainty analysis.

2.1 Engine Setup

The engine used is a GM EcoTec Turbo 2.0-liter LHU engine coupled to a 460 hp AC Dynamometer. The engine specifications are given in Table 2.1. Previous studies on this engine include research on Homogeneous Charge Compression Ignition (HCCI)

Table 2.1
Engine specifications

Make	General Motors
Model	Ecotec 2.0 L Turbocharged
Engine Type	4 Stroke, Gasoline
Fuel System	Direct Injection
No of Cylinders	4
Displaced Voulme	1998 [cc]
Bore	86 [mm]
Stroke	86 [mm]
Compression ratio	9.2:1
Max engine power	164 @ 5300 [kW@rpm]
Max engine torque	353 @ 2400 [Nm@rpm]
Firing order	1-3-4-2
IVO	25.5/-24.5 [°CAD bTDC]
IVC	2/-48 [°CAD bBDC]
EVO	36/-14 [°CAD bBDC]
EVC	22/-28 [°CAD bTDC]
Valve Lift	10.3 [mm]

[45] [46], Partially Premixed Compression Ignition (PPCI) [47], and Reactivity Controlled Compression Ignition (RCCI) [38] [44] [47]. The engine originally was a GDI engine but was modified to enable dual fuel operation. Two low pressure fuel rails were added to enable port fuel injection. More details about PFI injection systems can be found in previous works [42] [47]. The turbocharger was disabled and all the experiments in this thesis were carried out under naturally aspirated conditions. Two controllable air heaters were installed along the intake air stream so that the intake air temperature could be set to a desired value. The engine test setup schematic is shown in Figure 2.1 along with the locations of the thermocouples, pressure transducers and lambda sensors.
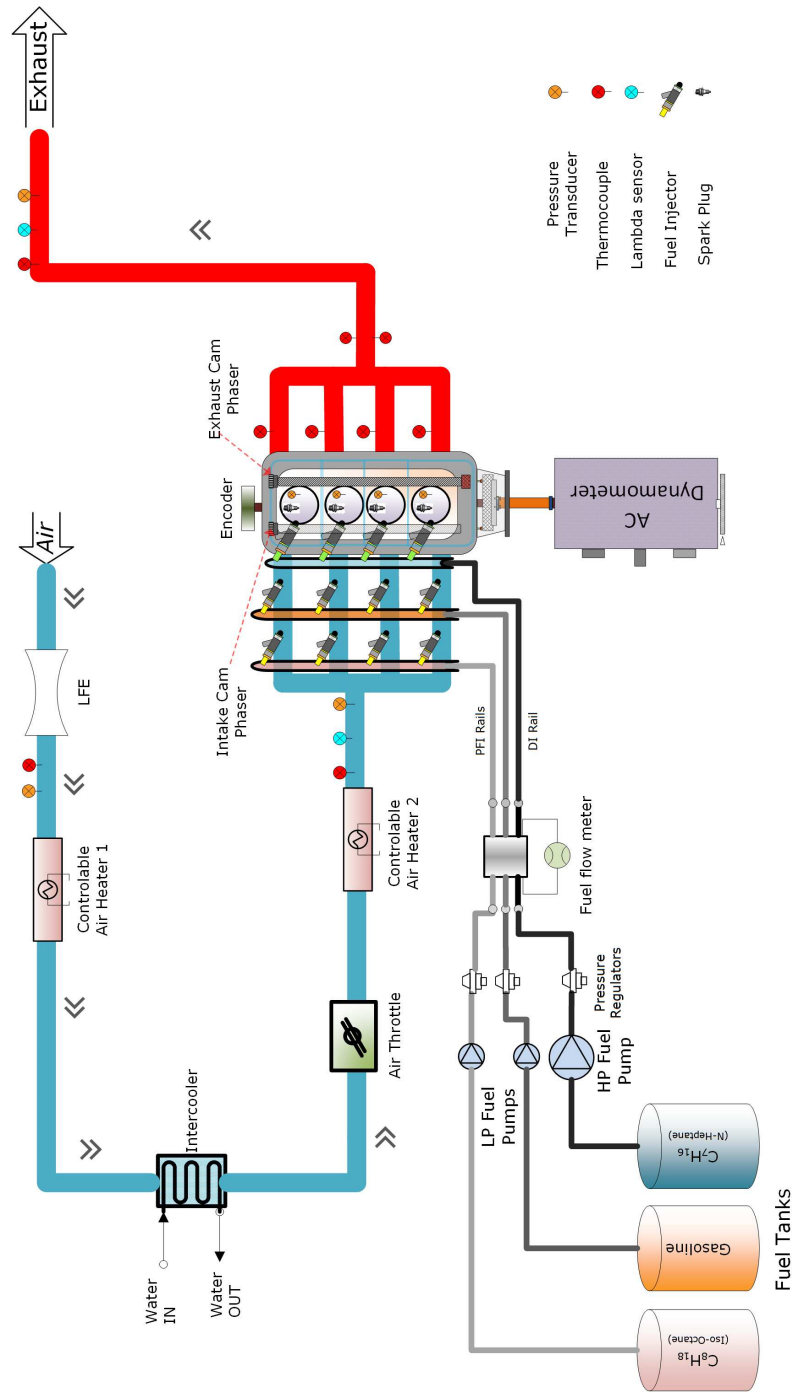
Figure 2.1: Engine Test Setup Schematic

2.2   Data Acquisition and Control

To control the engine, a dSPACE MicroAutoBox (MABX) was programmed to provide all required engine control unit (ECU) functions. To enable cycle-to-cycle combustion control, a Xilinx Spartan-6 Field Programmable Gate Array (FPGA) was programmed for real-time calculations of combustion metrics such as CA50, IMEP, heat release rate (HRR), and start of combustion (SOC). These calculations were carried out by feeding the pressure trace and encoder pulses through an I/O board. The specifications of the FPGA and the I/O board are given in Table 2.2. These combustion metrics were then fed to the real-time processor board of the MABX where the controller was embedded. The detailed description regarding calculations of the combustion metrics can be found in [44]. An overview of the MABX hardware is shown in Figure 2.2. In addition, the control setup uses a RapidPro® which is a slave processor/control unit that communicates with the MABX through CAN. RapidPro® contains modules for controlling actuators like spark plugs, port-fuel injectors, direct injectors, cam phasors, throttle valve and EGR valve and also for acquiring data from sensors like lambda sensor, crank position sensor and cam position sensor. Details regarding RapidPro® for the experimental setup in this study are found in [45].

The in-cylinder pressure was measured using four PCB Piezotronics 115A04 transducers. In this study, pressure data from only cylinder 1 is focused on. The specifications

Table 2.2
FPGA board and I/O Specification

	Component	Specification
FPGA	Xilinx Spartan-6 LX150	
	Logical cells (nos)	147443
	Slice registers (nos)	184304
	Slice LUT (nos)	92152
	Block RAM blocks (kB)	4824
	Clock speed(MHz)	80
I/O Board	dSPACE DS1552	
	A/D converter	
	Sampling frequency (MSPS)	1
	Resolution (Bit)	16
	Input (V)	± 10
	Digital input	
	Update rate (MHz)	80
	Input (V)	± 40
	Threshold level L $\Rightarrow$ H (V)	3.6
	Threshold level H $\Rightarrow$ L (V)	1.2

of the pressure transducer used in cylinder 1 are given in Appendix C. Encoder Products Company's crank shaft encoder, model no. 260, with resolution of 1 Crank Angle Degree (CAD) was used to measure the engine crank angle and RPM. A DSP Technology ACAP combustion analyser was used to monitor and post process combustion data (CA50, IMEP, peak pressure, etc).
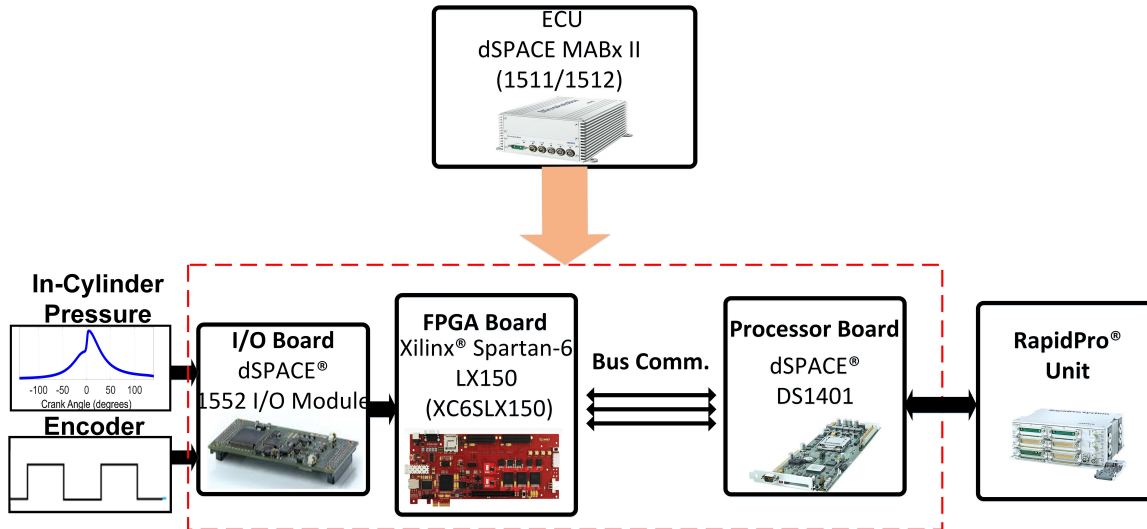
Figure 2.2: MicroAutoBox hardware overview for cycle by cycle combustion phasing control in this work

2.3 Test Procedure

RCCI is a type of dual-fuel combustion where-in a high reactivity fuel is directly injected into the cylinder while a low-reactivity fuel is injected via port-fuel injection. The high reactivity fuel used in this work is n-heptane, while the low reactivity fuel used is iso-octane. The properties of the fuels are given in Table 2.3

Table 2.3
Test fuel properties [48]

Property	n-heptane	iso-octane
Higher Heating Value[MJ/kg]	48.07	47.77
Lower Heating Value [MJ/kg]	44.56	44.30
Density [kg/m^3]	686.6	693.8
Octane Number [-]	0	100
H/C ratio [-]	2.29	2.25

N-heptane was injected using the high pressure DI fuel rail while iso-octane was injected using one of the low pressure PFI rails. Since the compression ratio of the test engine was low to facilitate cold start of RCCI combustion, initially the engine was run in SI mode by injecting gasoline using the other PFI fuel rail to heat up the engine. The amount of iso-octane and n-heptane injected was adjusted by a factor called Premixed Ratio (PR). PR is defined as the ratio of iso-octane energy equivalence to the total energy supplied by the fuel. PR is calculated by Equation (2.1) where LHV_n and LHV_i are the lower heating values of n-heptane and iso-octane, respectively.

$$PR = \frac{m_{iso}LHV_{iso}}{m_{iso}LHV_{iso} + m_{nhep}LHV_{nhep}} \tag{2.1}$$

Details regarding calculation of mass of fuels of the two fuels and injector pulse widths based on a PR input can be found in [47]. Two types of experiments were mainly conducted, including steady-state and transient tests. Steady-state data was used to parameterize the Mean Value Models that will be discussed in Chapter 3. Data for 100 cycles was recorded for combustion analysis. Points with a Coefficient of Variation (COV) of IMEP of over 5%[1] were discarded. The tests were run at a constant speed of 1000 RPM and a constant intake temperature of 60^oC. For a particular PR and start of injection (SOI), a fuel quantity sweep was conducted. The combination of PR and SOI in this study are defined by the test matrix in Table 2.4.

The data used for parameterization can be found in appendix A. For transient tests

---

[1]Measured using the data recorded by ACAP combustion analyzer.

Table 2.4

Steady state test matrix to obtain data for parameterizing mean value models at 1000 RPM and $T_{in} = 60^oC$, EGR=0% at naturally aspirated conditions

PR	SOI (CAD bTDC)	FQ (mg/cycle)
10	30	19-25
	35	20-25
	40	21-25
	45	21-25
	50	22-24
20	30	20-25
	35	21-25
	40	21-25
	45	23-26.5
30	35	22-25
	40	22-25
	45	22-25
	50	23-26
40	40	24-27
	45	23-27
	50	22-27
	55	22-25

used in chapters 3, 4 and 5, data was typically recorded for around 300 cycles.

2.4 Uncertainty Analysis of Measured and Derived Parameters

All measurements are subject to uncertainty mainly due to limited accuracy of the measuring apparatus. Since the accuracy can propagate into derived parameters

and affect the repeatability and reliability of results, it is essential to characterize

uncertainty in measure and calculated variables.

Table 2.5 provides a list of measured inputs with their range and their uncertainties.

Table 2.5
Measured input parameters and their uncertainties for the RCCI engine
experimental setup [47]

Parameter [Units]	Value	Uncertainty($\pm$)
Bore[m]	0.086	0.001
Stroke[m]	0.086	0.001
Length[m]	0.145	0.001
Cylinder Pressure[kPa]	95-4000	1%
Crank Angle[CAD]	0-720	1
λ[-]	1.0-3.0	0.05
T_{in}[°C]	40-100	2%
N[rpm]	800-2200	10
m_{air}[g/s]	12.1 - 31.0	0.72%
m_{fuel}[mg/cycle]	11.0-40.0	0.1%
P_{in}[kPa]	95-105	0.5%
$T_{exhaust}$[°C]	350-700	2%

The uncertainty in measured parameters is propagated into the derived parameters.

If a derived variable is a function of multiple measured variables then, the uncertainty

propagation is calculated by Equation (2.2) [49]:

$$U_y = \sqrt{\sum_i \left(\frac{\partial Y}{\partial X_i}\right)^2 U_{X_i}^2} \qquad (2.2)$$

where, Y is the derived variable, X_i are the measured variables; and U_y and U_X are

the uncertainties in derived and measured variables, respectively. Table 2.6 shows the

uncertainty analysis conducted for the engine and experimental steup in this study.

Table 2.6

Uncertainties of derived parameters from measured variables for the RCCI
engine experimental setup in this thesis [38]

Derived parameter [Units]	Value± Uncertainty
BD [CAD]	6±1
CA50 [CAD aTDC]	-1±1
IMEP [kPa]	540.7±28.1

Chapter 3

RCCI Dynamic Modelling

3.1 Modelling Introduction

For model-based real-time combustion and load control, a plant model is required. This plant model should be computationally efficient yet accurate enough that it could be utilized for closed-loop combustion control. Over the years various plant models have been developed for compression ignition (CI) engines, ranging from complex CFD models [17] [50] [51] to simple physics-based control-oriented models (COM) [40] [42]. CFD models although accurate are computationally intensive and thus cannot be used for real-time combustion control. Prior studies on developing simple COMs to predict combustion phasing in HCCI [52] [53] and RCCI [42] have shown that they

combine computational efficiency with required accuracy for control applications.
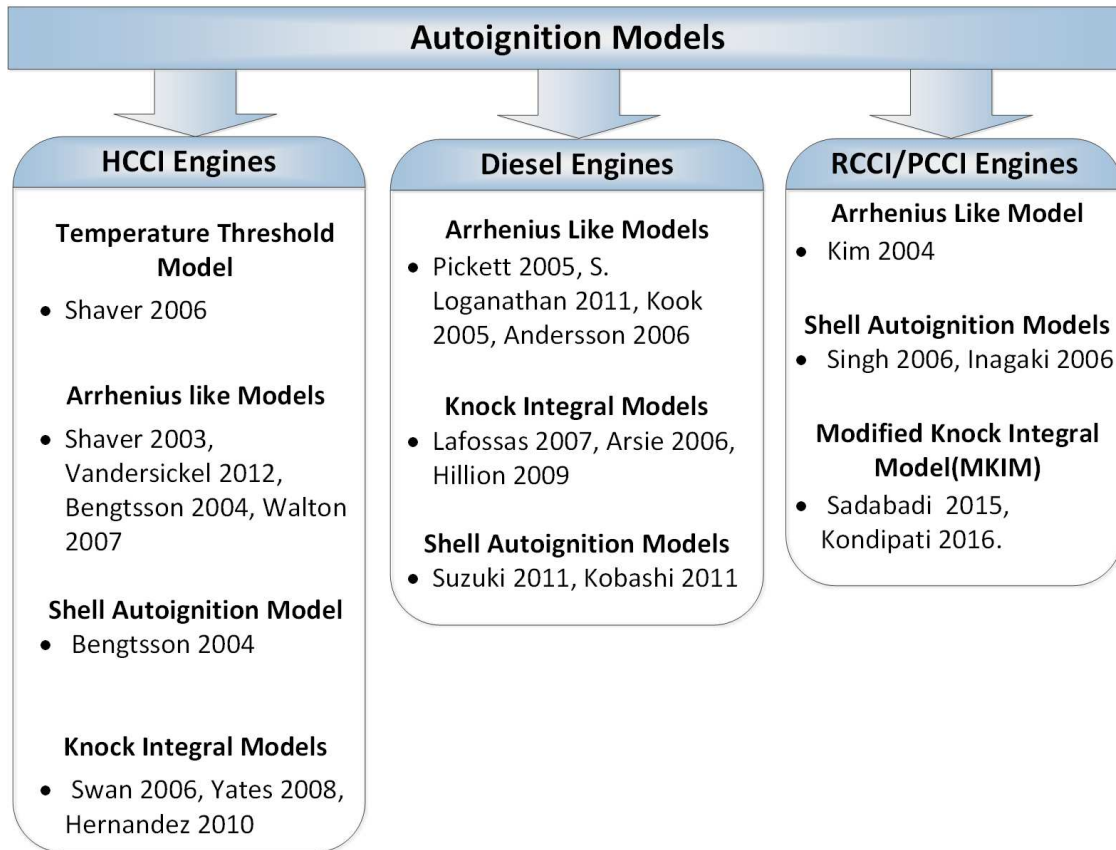
Figure 3.1: Control-oriented autoignition models for compression ignition engines [38] [42] [54] [55] [56] [57] [58] [59] [60] [61] [62] [63] [64] [65] [66] [67] [68] [69] [70]

Figure 3.1 lists some of the previous studies in developing COMs for CI combustion. COMs such as Arrhenius-like models [55] [56] [57] [59] and Shell auto-ignition models [62] [63] [64] have been widely used for predicting SOC in diesel as well as HCCI combustion. The Knock Integral Model (KIM) was originally developed by Livengood et al. [71] for predicting the onset of knock in SI engines. Hillion et al. [67], Arsie et al. [69] used the KIM to predict SOC in diesel combustion. Shahbakhti and Koch [72] used this model to predict SOC in HCCI combustion. Sadabadi and Shahbakhti

24

[73] developed a COM by modifying the KIM for predicting SOC in RCCI combustion. This COM was parameterized using the data obtained from KIVA simulations. Kondipati [38] then used experimental RCCI engine data to parametrize the COM to predict SOC in RCCI engines. This work uses the Modified Knock Integral Model (MKIM) developed by Sadabadi and Shahbakhti [42] and the modified Weibe model developed by Kondipati [38]. The MKIM is less accurate as compared to the shell auto-ignition model for predicting SOC. However it is computationally more efficient. These Mean Value Models (MVMs) are used to predict the steady-state SOC and CA50, respectively. MVMs are then combined with physics-based equations to include transient dynamics operation in RCCI engines. In this chapter, new models are developed to calculate the IMEP, and to account for residual gas thermal dynamics and fuel dynamics. The dynamic model developed is then simplified further and linearized for RCCI controller design. The following sections explain the development of the COM in detail.

3.2 Start of Combustion (SOC)

3.2.1 Modified Knock Integral Model (MKIM)

Livengood et al. [71] developed the Knock Integral Model to predict auto-ignition in SI engines. Later it was modified by Shahbakhti and Koch [72] to predict auto-ignition in HCCI engines. Sadabadi [42] extended the MKIM to include RCCI combustion by dividing the model into two stages; the first stage is from intake valve closing (IVC) to start of injection (SOI) which deals with the compression of the port fuel injected low reactivity fuel (iso-octane). The second stage is from SOI to IVC which deals with the compression of the mixture of high and low reactivity fuels and the onset of auto-ignition.

$$
\int_{SOI}^{SOC} \frac{d\theta}{A_2 N \left(\phi_{DI}^{B_{2DI}} + \phi_{PFI}^{B_{2PFI}} \right) exp\left(\frac{\frac{C_2}{CN_{mix}+b}(P_{ivc}v_c^{nc})^{D_2}}{T_{ivc}v_c^{nc-1}} \right)} +
$$
$$
\int_{IVC}^{SOI} \frac{d\theta}{A_1 N \phi_{PFI}^{B} exp\left(\frac{C_1(P_{ivc}v_c^{nc})^{D_1}}{T_{ivc}v_c^{nc-1}} \right)} = 1 \tag{3.1}
$$

Where N is the engine speed, P_{ivc} and T_{ivc} are the pressure and temperature at intake valve closing conditions, respectively. ϕ_{DI} and ϕ_{PFI} are global equivalence ratios of

n-heptane and iso-octane respectively calculated by using the following equations:

$$\phi_{DI} = (1 - PR).\phi_{tot} \tag{3.2a}$$

$$\phi_{PFI} = PR.\phi_{tot} \tag{3.2b}$$

Where ϕ_{tot} is the global combined equivalence ratio.

Since IVC occurs at 2 CAD before BDC, P_{ivc} and T_{ivc} are taken to be equal to the manifold pressure and temperature. CN_{mix} in Equation (3.2) is the Cetane Number and is used to account for the reactivity of the fuel mixture. The CN of the mixture is given by Equation (3.3) where $FAR_{st,nhep}$ and $FAR_{st,iso}$; CN_{iso} and CN_{nhep} are stoichiometric fuel-air ratios and cetane numbers of n-heptane and iso-octane, respectively.

$$CN_{mix} = \frac{\left(FAR_{st,nhep}\phi_{DI}CN_{nhep} + FAR_{st,iso}\phi_{PFI}CN_{iso}\right)}{FAR_{st,nhep}\phi_{DI} + FAR_{st,iso}\phi_{PFI}} \tag{3.3}$$

n_c in Equation (3.2) is the polytropic compression coefficient which is the slope of the compression stroke on the PV diagram. v_c is the ratio of the volume at IVC to the volume at any instant.

$$v_c = \frac{V_{IVC}}{V(\theta)} \tag{3.4}$$

$A_1, A_1, B, B_{2DI}, B_{2PFI}, b, C_1, C_2, D_1, D_2$ are constants which are estimated using the parametrization data from Chapter 2.

3.2.2 Parameterization of MKIM

To parametrize and validate the MKIM model, 47 steady-state operating points were recorded. 24 points were used for parameterizing the MKIM, while the rest of the data points were used to validate the model. The data points were taken at a constant 1000 RPM and intake temperature of 60 ^{o}C. The operating conditions of the experimental data points are given in Table 3.1. Previous work by Kondipati [38] used an iterative optimization approach to calculate the parameters of the MKIM. This work uses the same approach by using the $fminsearch$ command in MATLAB®. This command uses the Nelder-Mead simplex optimization method [74] to reduce the error between the estimated SOC and the experimental SOC. The optimized parameters are given in Table 3.2.

Table 3.1
Operating engine conditions for estimation and validation of the MKIM model

Parameter [Units]	Operating value
PR [-]	10-20-30-40
SOI [CAD bTDC]	30-40-50-60
T_{in} [°C]	60
λ [-]	2.5-1.0
P_{in} [kPa]	96.5
IVO [CAD bTDC]	25.5
EVC [CAD bTDC]	22
Speed [RPM]	1000

,

28

Table 3.2
Optimized parameters for the MKIM model

A_1	B	C_1	D_1	A_2
0.5366	-0.0072	5.2104	-0.0002	0.0024
B_{2DI}	B_{2PFI}	C_2	b	D_2
0.0016	7.3403e-05	1512.17e+03	174.24	-0.2374

Figure 3.2 shows the SOC estimation results along with the average experimental SOC (diamond symbols) and the range of cyclic data for 100 cycles recorded for each operating point. It can be seen that the SOC can be estimated with an average error of 1.8 CAD. e_{ave} and σ_e show the average and standard deviation of errors, respectively. The estimated parameters were then used to calculate the SOC for 23 steady-state data points different from those used to estimate the MKIM parameters. Figure 3.3 shows the validation results. The average error is 1.9 CAD which is sufficient for RCCI combustion control.
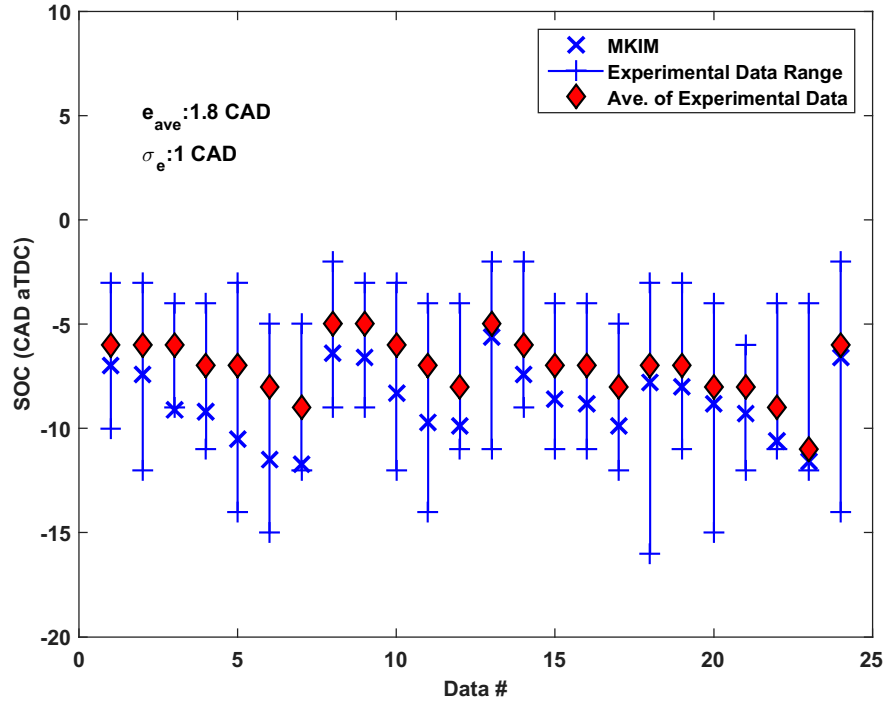
Figure 3.2: Estimation of MKIM parameters using 24 steady-state operating points
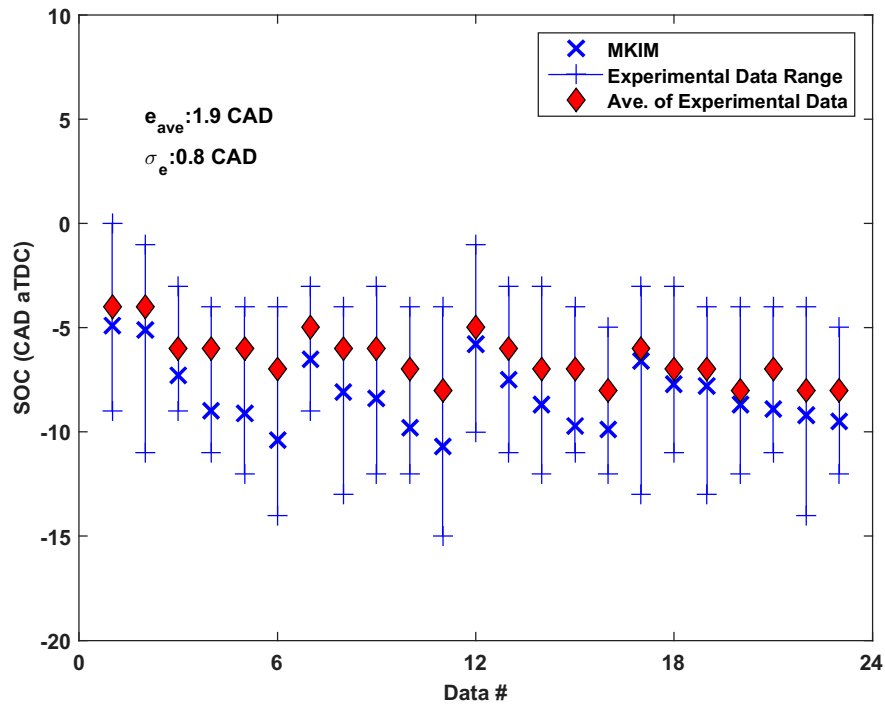
Figure 3.3: Validation of MKIM model using 23 steady-state operating points

3.3 Combustion Phasing (CA50) Model

3.3.1 Modified Weibe Model

Combustion phasing is one of the main parameters which characterize RCCI combustion; thus, combustion phasing and hence is an important control parameter to achieve high efficiency RCCI operation [47]. Sadabadi [42] developed a modified Weibe function to calculate CA50 using the mass fraction burned (x_b) in RCCI combustion. CA50 is taken as the crank angle at which x_b reaches 0.5. Here, x_b is calculated using the RCCI modified Weibe model from [42]:

$$x_b(\theta) = 1 - exp\left(-A\left[\frac{\theta - \theta_{soc}}{\theta_d}\right]^B\right) \qquad (3.5)$$

where, θ_{soc} is SOC predicted from the MKIM. θ_d is the burn duration given by Equation (3.6).

$$\theta_d = C(1 + X_d)^D.(\phi_{DI}^E + \phi_{PFI}^F) \qquad (3.6)$$

X_d is the dilution fraction which accounts for the EGR and residual gases. ϕ_{DI} and ϕ_{PFI} are the global equivalence ratios of n-heptane and iso-octane, respectively given by Equation (3.2). A, B, C, D, E, F are constants which are estimated using the experimental data.

3.3.2 Parametrization of CA50 model

To paramterize the CA50 model, a similar approach to Section 3.2.2 was used. 24
steady state operating points were used to parameterize the model and 23 operat-
ing points, different from the ones used for parameterization, were used to validate
the CA50 model. The parameterization was done using the Nelder-Mead Simplex
algorithm [74]. The optimized parameters are listed in Table 3.3.

Table 3.3
Optimized parameters for the CA50 model

A	B	C
0.1073	14.952	6.5361
D	E	F
0.03813	-0.1726	0.1064

The results of the 24 points used for parameterization are shown in Figure 3.4. It can
be seen that the average error between predicted and experimental values of CA50 is
1 CAD. The validation results are shown in Figure 3.5. The validation results confirm
that the model is able to predict the CA50 with an average error of 1 CAD. This
error is minimal; thus, the CA50 model can be used for RCCI controller design.
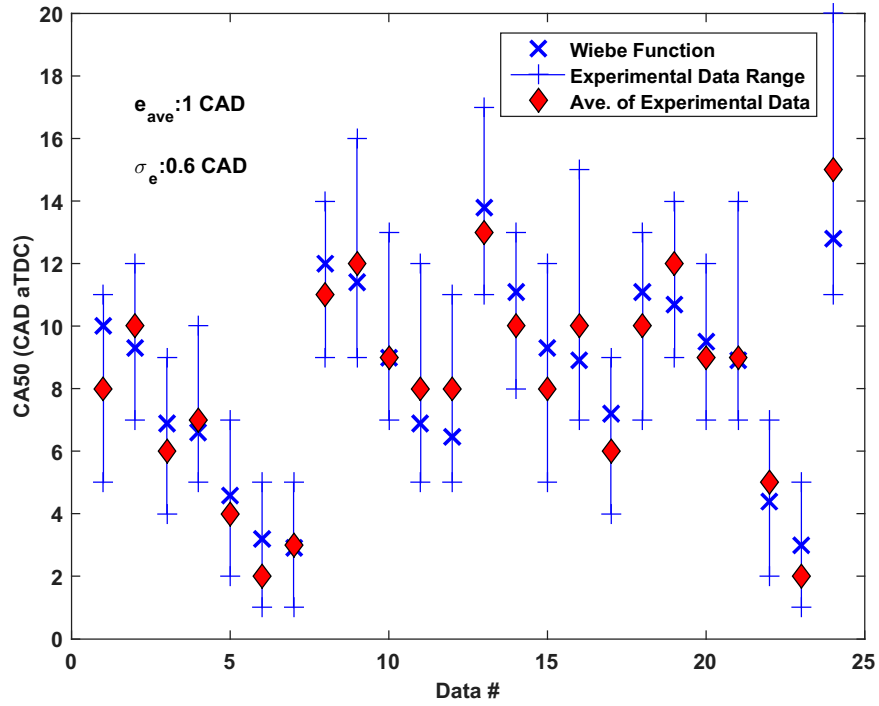
Figure 3.4: Estimation of CA50 parameters using 24 steady-state operating points
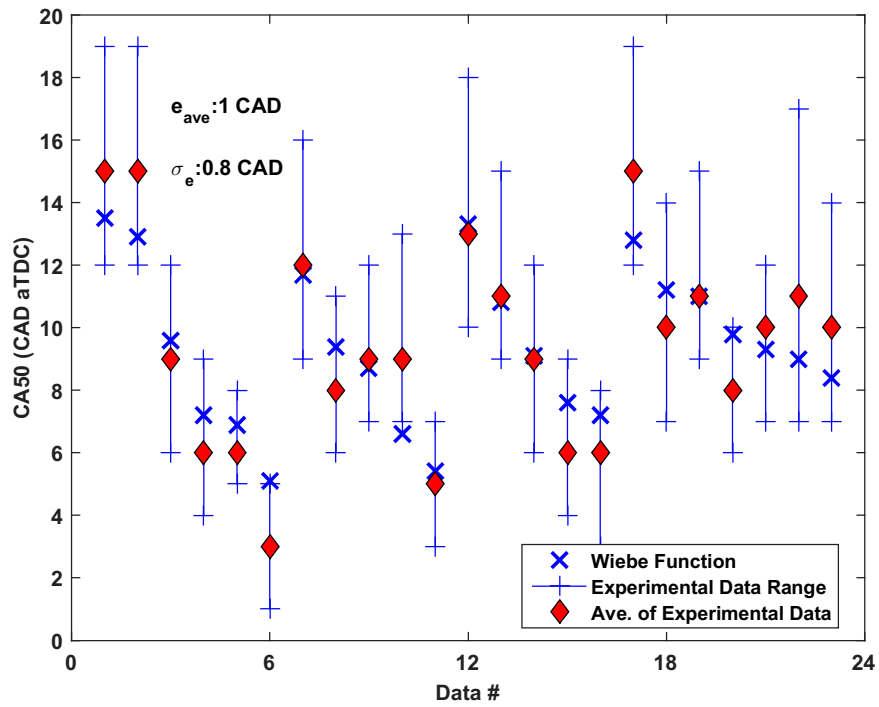
Figure 3.5: Validation of CA50 model using 23 steady-state operating points

33

3.4   Dynamic Model

In order to control transient operation of the engine on a cycle-to-cycle basis, a control oriented model is developed to predict the metrics of the RCCI engine cycle. Hence the mean value models developed in Sections, 3.2 and 3.3 are extended to include the entire cycle from intake valve opening to exhaust valve closing. In addition, the effect of the previous engine cycle on the combustion of the current cycle is taken into account by including the effect of mixing of the residual gases trapped at the end of the previous cycle with the fresh charge from the current cycle.

3.4.1   Intake Stroke $(IVO \to IVC)$

The dynamic model is initialized with operating parameters including engine speed, PR, SOI, T_{in}, ϕ_{tot}, and the exhaust pressure (P_{exh}). In Section 3.2 it was assumed that P_{ivc} and T_{ivc} are equal to the manifold pressure and temperature respectively since IVC occurs close to BDC at 2 CAD before BDC. However, the temperature of the residual gases greatly affects T_{ivc} and in turn affects the SOC and combustion phasing. The mixing temperature at IVC is calculated by Equation (3.7), where X_{rg} is the residual gas mass fraction. $T_{rg,k}$ is the residual gas temperature of the previous

cycle and $T_{in,k+1}$ is the intake manifold temperature of the current cycle.

$$T_{ivc,k+1} = (1 - X_{rg})T_{in,k+1} + X_{rg}T_{rg,k} \tag{3.7}$$

For the first cycle it is essential to estimate the value of T_{rg} in order to initialize the model. Cavina [75] developed a model for estimating the residual gas fraction. This model is used to estimate the value of X_{rg} in this work.

$$X_{rg} = \sqrt{\frac{1}{C} \cdot \frac{\pi \cdot \sqrt{2}}{360} \cdot \frac{r_c - 1}{r_c} \cdot \frac{OF}{N} \sqrt{\frac{R.T_{in}|P_{exh} - P_{in}|}{P_{exh}}} \cdot \left(\frac{P_{exh}}{P_{in}}\right)^{\frac{\gamma+1}{2\gamma}}} + \frac{1}{C} \cdot \frac{r_c - 1}{r_c} \phi_{tot} \frac{V_{ivo}}{V_{dis}} \left(\frac{P_{exh}}{P_{in}}\right)^{\frac{1}{\gamma}} \tag{3.8}$$

Where, r_c is the compression ratio and OF is the overlap factor of the intake and exhaust valves. P_{exh} is the exhaust pressure, T_{in} and P_{in} are the intake manifold temperature and pressure, respectively. R is the gas constant. V_{ivo} and V_{dis} are the volume at intake valve closing and displaced volume, respectively. k is the ratio of specific heats. C is given by:

$$C = \left[1 + \frac{LHV}{c_v T_{in}(\frac{m_{tot}}{m_f}).r_c^{\gamma-1}}\right]^{\frac{1}{\gamma}} \tag{3.9}$$

where c_v is the specific heat capacity at constant volume at IVC condition and LHV is the lower heating value of the fuel mixture given by

$$LHV = \frac{PR}{100}.LHV_{iso} + \left(1 - \frac{PR}{100}\right).LHV_{nhep} \qquad (3.10)$$

The X_{rg} from Equation (3.8) is used to initialize the engine cycle. Then at the end of the current cycle, the X_{rg} is re-calculated using Equation (3.11). Next, an iterative loop is carried out until the value of X_{rg} converges to a terminal value. In a similar way, T_{rg} is re-calculated at the end of the cycle and an iterative loop is used to converge to a terminal value.

$$X_{rg} = \frac{m_{rg}}{m_{tot}} \qquad (3.11)$$

Where, m_r is the mass of the residual gasses and m_{tot} is the total mass of mixture inside the cylinder at IVC. m_{rg} is calculated based on exhaust valve closing (EVC) conditions as will be explained in subsequent sections.

3.4.2 Polytropic Compression $(IVC \rightarrow SOC)$

By assuming the compression to be polytropic [76], the pressure at SOC (P_{soc}) and temperature at SOC (T_{soc}) are calculated by the Equations (3.12) and (3.13). For using these equations, the SOC needs to be deterimined. This is done by using the

MVM developed in Section 3.2.1.

$$T_{soc,k+1} = T_{ivc,k+1} \left(\frac{V_{ivc}}{V_{soc,k+1}} \right)^{n_c-1} \tag{3.12}$$

$$P_{soc,k+1} = P_{ivc,k+1} \left(\frac{V_{ivc}}{V_{soc,k+1}} \right)^{n_c} \tag{3.13}$$

Where, n_c is the polytropic coefficient calculated from the experimental data. V_{ivc} and V_{soc} are the volumes at IVC and SOC, respectively.

3.4.3   Combustion $(SOC \rightarrow EOC)$

CA50 is predicted by using the CA50 model developed in Section 3.3. End of combustion (EOC) is predicted by using the following Burn Duration (BD) model.

3.4.3.1   BD Model for EOC state estimation

In RCCI combustion, the primary combustion mechanism is through spontaneous ignition front since the charge is incapable of sustaining flame propagation [50]. Sadabadi [42] developed a correlation to link the spontaneous ignition front speed (S_{ig}) with the burn duration as follows:

$$BD = K_2 (S_{ig})^t \tag{3.14}$$

37

Where, K_2 and t are parameters to be estimated. The introduction of the high reactive fuel creates fuel stratification and combustion starts in pockets rich in high reactivity fuel. Thus the ignition delay is not constant throughout the chamber. Sadabadi [42] proposed using the following equation to calculate the ignition front speed in RCCI combustion:

$$S_{ig} = \frac{1}{|\frac{d\tau}{d\phi_{DI}}||\nabla\phi_{DI}|} \tag{3.15}$$

Where, τ is the ignition delay which is given by the denominator of MKIM Equation (3.1) from SOI to SOC period. The gradient of equivalence ratio is given by:

$$|\nabla\phi_{DI}| = \frac{K_1}{ID^p}.\phi_{DI}^r \tag{3.16}$$

where ID refers to ignition delay and is calculated by using:

$$ID = SOI - SOC \tag{3.17}$$

Once BD is estimated, EOC is calculated by using Equation (3.18):

$$EOC = SOC + BD \tag{3.18}$$

The temperature rise during combustion is calculated by [42]:

$$\triangle T = \frac{LHV_{DI}(F/A)_{st,nhep}.\phi_{DI} + LHV_{PFI}.(F/A)_{st,iso}.\phi_{PFI}}{c_v((F/A)_{st,nhep}.\phi_{DI} + (F/A)_{st,iso}.\phi_{PFI} + 1)} \tag{3.19}$$

A factor e_1 is introduced to account for heat losses during combustion. The factor e_1 can be assumed to be a second degree polynomial [77]. Thus the temperature at the end of combustion (EOC) can be given by:

$$T_{eoc,k+1} = T_{soc,k+1} + e_1.\Delta T \tag{3.20}$$

Similarly the pressure at the end of combustion is estimated by using the following equation.

$$P_{eoc,k+1} = P_{soc,k+1} + e_2.\Delta T \tag{3.21}$$

The factors e_1 and e_2 are determined by:

$$e_1 = a_0 + a_1\theta_{soc} + a_2\theta_{soc}^2 \tag{3.22}$$

$$e_2 = b_0 + b_1\theta_{soc} + b_2\theta_{soc}^2 \tag{3.23}$$

where $a_0, a_1, a_2, b_0, b_1, b_2, p, r, K_1, K_2$ and t are constants to be estimated. These parameters are estimated using the same optimization method used for parameterizing the MKIM and CA50 model. The final optimized parameters are given in Table 3.4.

Table 3.4
Optimized parameters for the BD model

K_1	t	K_2	a_0	a_1	a_2
4.254	-0.3347	32.6389	0.2152	-1.2389e-05	4.1071e-07

b_0	b_1	b_2	p	r
12.42655	0.001407	-3.3397e-05	2.2201e-05	0.53812

3.4.4 Polytropic Expansion $(EOC \rightarrow EVO)$

The expansion process can be modeled as a polytropic process [76]. The temperature and pressure at exhaust valve opening (EVO) can be calculated using the following polytropic equations:

$$T_{evo,k+1} = T_{eoc,k+1}\left(\frac{V_{eoc,k+1}}{V_{evo}}\right)^{n_e-1} \tag{3.24}$$

$$P_{evo,k+1} = P_{eoc,k+1}\left(\frac{V_{eoc,k+1}}{V_{evo}}\right)^{n_e} \tag{3.25}$$

Where n_e, is the polytropic expansion coefficient calculated from the experimental data. P_{evo} and T_{evo} are the pressure and temperature at the EVO condition, respectively.

3.4.5 Exhaust Stroke $(EVO \rightarrow EVC)$

The exhaust process can be approximated to be a polytopic process [42] and the temperature at EVC can be given by:

$$T_{evc,k+1} = T_{evo,k+1}\left(\frac{P_{exh,k+1}}{P_{evo,k+1}}\right)^{\frac{(n_e-1)}{n_e}}. \tag{3.26}$$

where P_{ex} is the exhaust pressure. The residual gas temperature is assumed to be equal to the T_{evc}. The mass of the residual gases (m_r) is calculated by using the ideal gas law for the EVC conditions

$$m_{evc,k+1} = \frac{P_{exh,k+1}.V_{evc}}{R_{evc}.T_{rg,k+1}}, \tag{3.27}$$

Where, R_{evc} is the gas constant. The residual gas fraction is calculated by:

$$X_{rg,k+1} = \frac{m_{evc,k+1}}{m_{tot,k+1}}. \tag{3.28}$$

The schematic of the entire RCCI dynamic model is summarized in Figure 3.6.
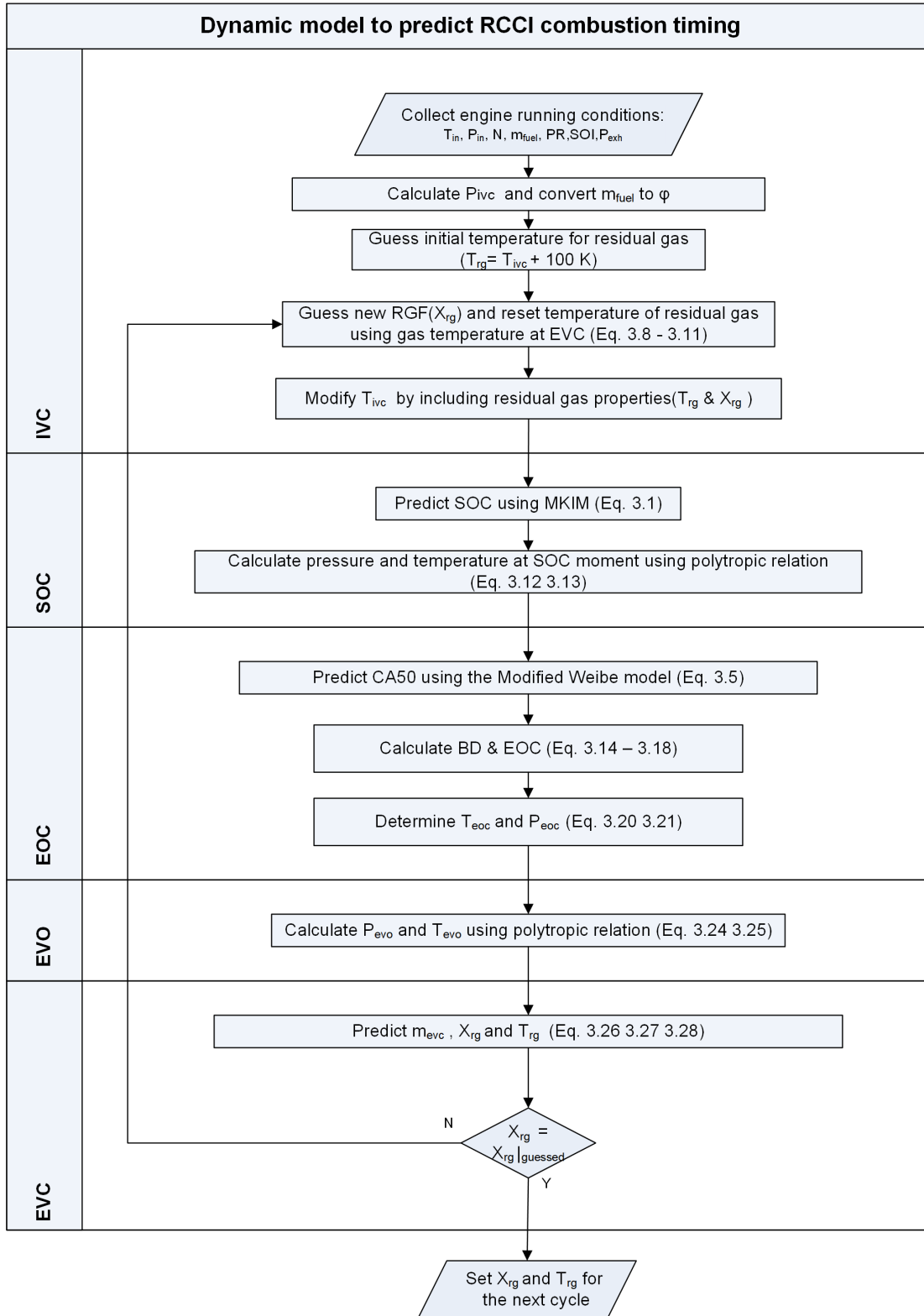
Figure 3.6: Dynamic Model of the RCCI engine cycle

3.5 IMEP Model

The dynamic model is extended to include IMEP to enable development of engine load controller. IMEP is calculated using the cyclic integral of the pressure trace times the volume given by Equation (3.29).

$$IMEP = \frac{1}{V_{dis}} \oint_V PdV \qquad (3.29)$$

However, accurate prediction of the pressure trace is difficult and computationally intensive. Bidarvatan [53] proposed using the temperature variations to calculate IMEP using the Equation (3.30). This work uses the same approach.

$$IMEP_{k+1} = m_{t,k+1} \frac{c_v}{V_{dis}} (T_{ivc,k+1} - T_{soc,k+1} + T_{eoc,k+1} - T_{evc,k+1}) \qquad (3.30)$$

Figure 3.7 shows the validation results of the IMEP model using the 23 steady-state experimental data points.
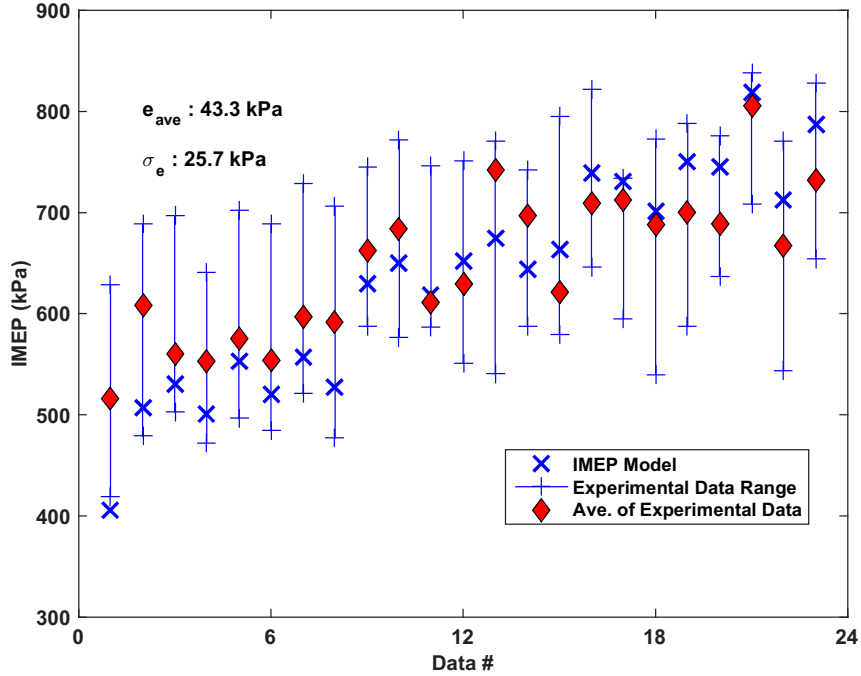
Figure 3.7: Validation of the IMEP model against the 23 steady-state operating conditions

3.6 Fuel Transport Dynamics

The fuel injected from the PFI injectors undergoes transport dynamics before going inside the cylinder. This becomes important for PR control during engine transients. Here, fuel transport dynamics are modeled using the $x - \tau_f$ model from [52] and [78]. This model assumes that the total injected fuel ($\dot{m}_{fi}$) into the intake ports gets divided into two parts. A fraction x is deposited onto the surface of the intake ports in the form of a thin liquid film, while the remaining part $(1 - x)$ is present in the form of vapor. Thus the fuel entering the cylinder is in two parts; fuel entering as

44

liquid due to the fuel film ($\dot{m}_{ff}$) and fuel entering into the cylinder in the vapor phase ($\dot{m}_{fv}$). The fuel entering the cylinder through the film is directly proportional to the mass of the fuel in the film and inversely to the time constant (τ_f). Thus the total fuel entering the cylinder ($\dot{m}_f$) is determined by the following equations:

$$\dot{m}_f = \dot{m}_{fv} + \dot{m}_{ff} \tag{3.31}$$

$$\dot{m}_{fv} = (1 - x)\dot{m}_{fi} \tag{3.32}$$

$$\ddot{m}_{ff} = \frac{x\dot{m}_{fi} - \dot{m}_{ff}}{\tau_f} \tag{3.33}$$

Other dynamics include the measurement dynamics of the lambda sensor and the transport delay caused due to the time it takes for the injected fuel to reach the lambda sensor. The measurement dynamics and the transport delay can be represented by a first order pole with a time constant of τ_m and a pure delay ΔT_m, respectively. Putting together the three dynamics discussed above yields:

$$\frac{\dot{m}_{fm}(s)}{\dot{m}_{fi}(s)} = \frac{1 + \tau_f(1 - x)s}{1 + \tau_f s} \frac{K_p}{1 + \tau_m s} e^{-s\Delta T_m} \tag{3.34}$$

where, $\dot{m}_{fm}$ is the fuel flow calculated using the lambda sensor measurements.

3.6.1 Model Parameterization

3.6.1.1 AFR sensor time constant and exhaust transport delay

When PR is set to zero, the entire fuel mass is injected from the DI fuel injector. Thus there is no dynamics caused by the fuel film formation in the intake ports. The fuel dynamics at this condition can be modeled simply by a single pole with delay as follows.

$$\frac{\dot{m}_{fm}(s)}{\dot{m}_{fi}(s)} = \frac{K_p}{1 + \tau_m s} e^{-s \Delta T_m} \tag{3.35}$$

By using system identification methods, ΔT_m and τ_m are obtained by giving a step change to the fuel quantity. The resulting identified parameters are $\Delta T_m = 0.15 sec$ and $\tau_m = 0.43 sec$. Figures 3.8, 3.9 and 3.10 shows the comparison between input λ^1, the λ with included lag effect, and the measured λ.

3.6.1.2 Fuel film dynamics

Using the parameters estimated in Section 3.6.1.1, x and τ_f are estimated by giving a step change to the fuel quantity at PR 20 and PR 40. Figures 3.9 and 3.10 show the estimation results at PR 20 and PR 40, respectively.

---

[1] λ is the ratio of actual AFR to the stoichiometric AFR
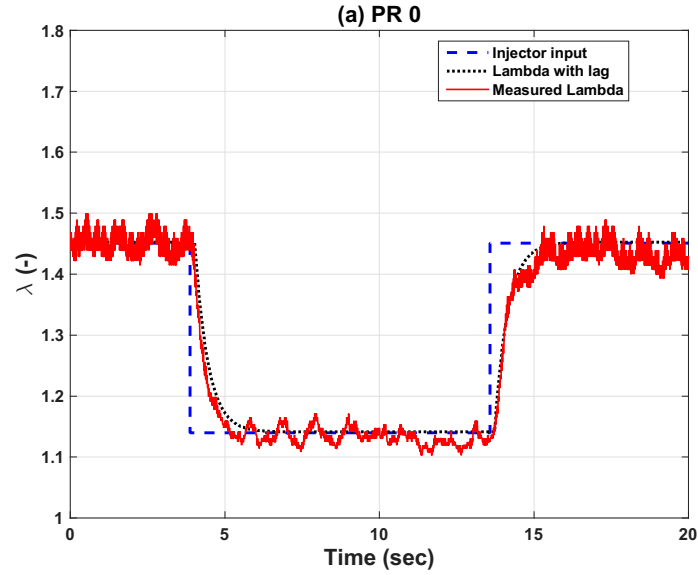
Figure 3.8: Measured and estimated *Lambda* with included lag effect, N=1000 RPM, $T_{in} = 60^{o}C$, PR=0. No fuel film dynamics are present here; thus $X = 0$.
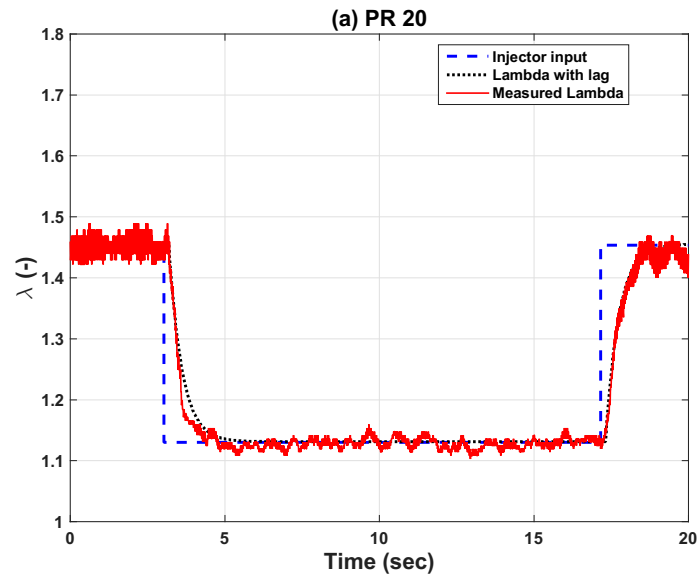
Figure 3.9: Measured and estimated *Lambda* with included lag effect, N=1000 RPM, $T_{in} = 60^{o}C$, PR= 20. The identified parameters are $x = 0.095$ and $\tau_f = 0.06sec$
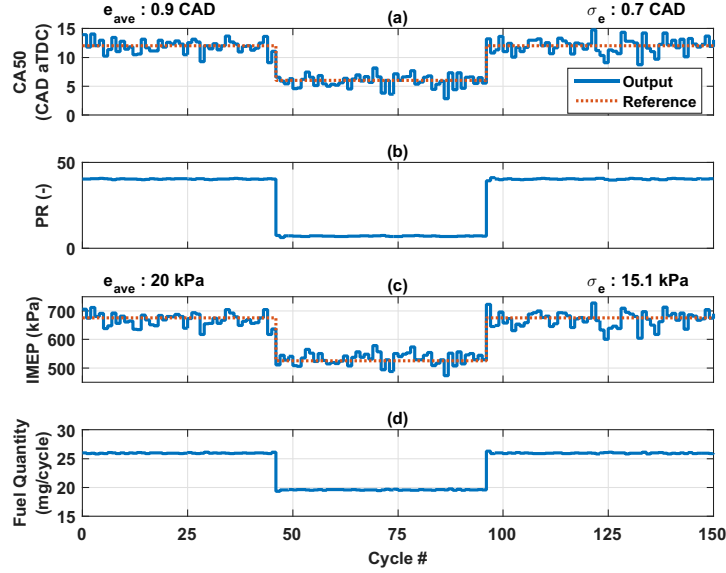
Figure 3.10: Measured and estimated AFR with lag , N=1000 RPM, $T_{in} = 60^oC$, PR=40. The identified parameters are $x = 0.195$ and $\tau_f = 0.16sec$

3.7 Validation of the Dynamic RCCI Model

To develop the dynamic model, some assumptions were made. Hence it is imperative to validate the dynamic model with experimental data. This is done by subjecting the dynamic model to transient experiments and then compare the output with experimental results. The following section discusses the effect of giving step inputs to PR, SOI and FQ in separate tests. To account for measurement noise in experimental results a measurement noise of standard deviation of 1.1 CAD and 23 kPa was added to the outputs of the dynamic model.

3.7.1 PR Step Transient Validation

Figure 3.11 shows the performance of the dynamic model when the engine is undergoes a step change in PR. We can see that as the PR is increased, the CA50 gets retarded. The dynamic model is able to predict CA50 with an average error of 1.6 CAD and predicts the IMEP with an average error of 36 kPa.
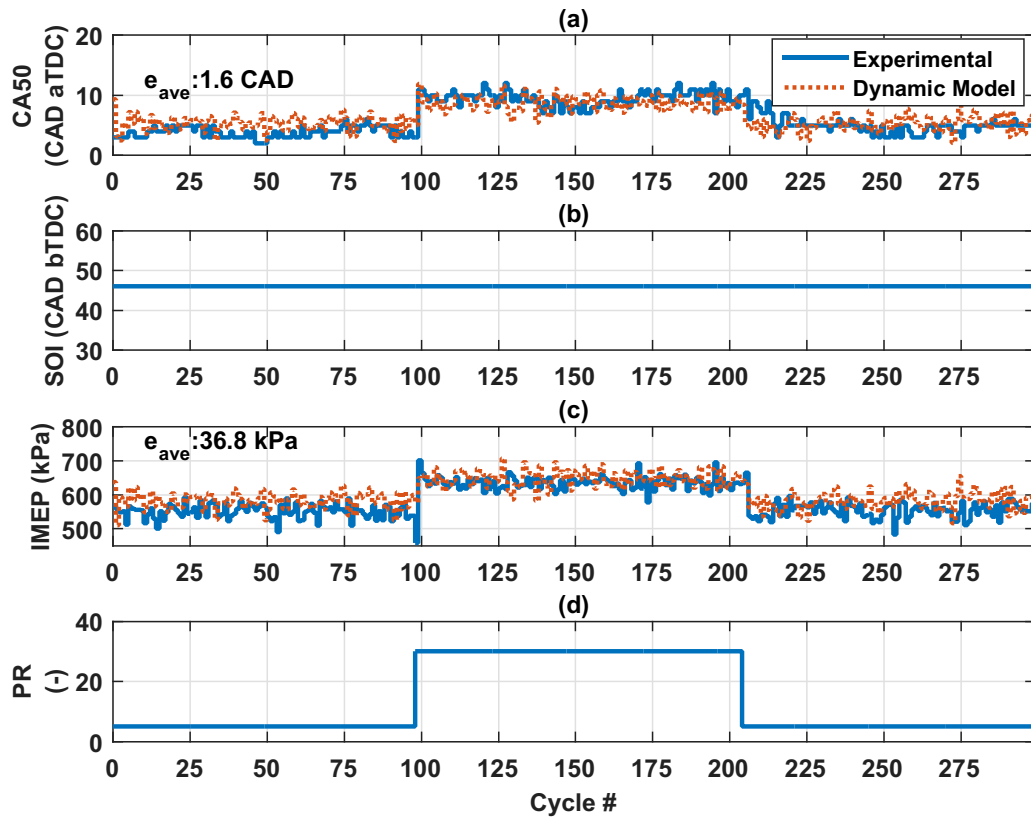
Figure 3.11: Validation of the dynamic model with experimental results for varying PR, N=1000 RPM, $T_{in} = 60^oC$, SOI= 50 CAD bTDC, FQ= 23 mg/cycle.

3.7.2 SOI Step Transient Validation

Performance of the developed dynamic model is also assessed when the RCCI engine undergoes a step change in SOI, as shown in Figure 3.12. We can see that as the SOI is retarded, the CA50 gets retarded. The dynamic model is able to predict CA50 with an average error of 1.8 CAD and the IMEP with an average error of 28.2 kPa.
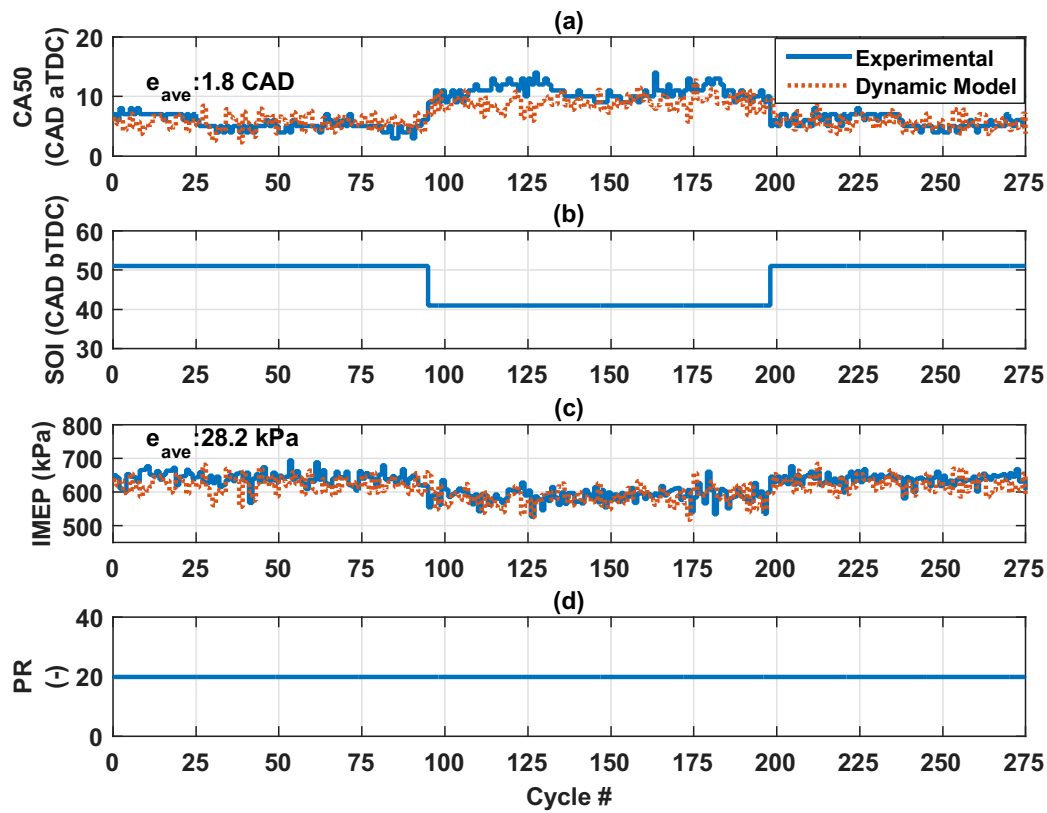
Figure 3.12: Validation of the dynamic model with experimental results for varying SOI, N= 1000 RPM, $T_{in} = 60^oC$, PR= 20, FQ= 23 mg/cycle

3.7.3 FQ Step Transient Validation

Experimental validation of the dynamic model for a step change in total fuel quantity (FQ) is shown in Figure 3.13. We can see that as the injected FQ is increased, the IMEP increases while the CA50 remains almost unchanged. The dynamic model is able to predict CA50 with an average error of 2.6 CAD and the IMEP with an average error of 43.3 kPa.
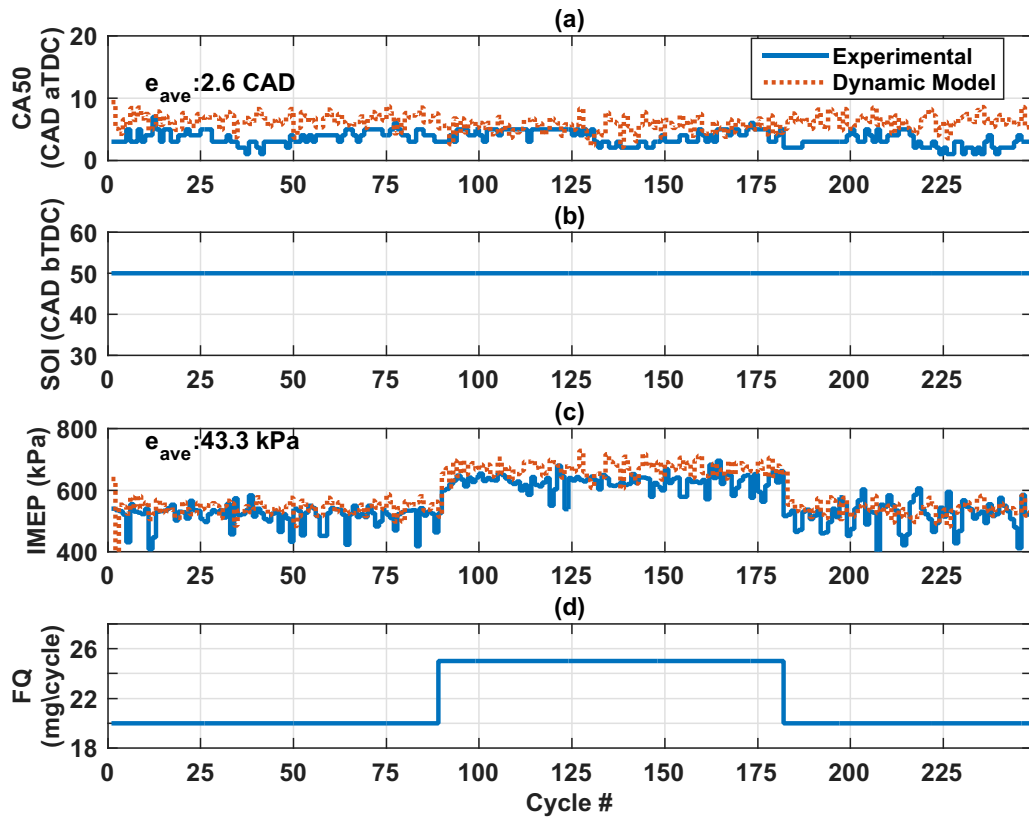
Figure 3.13: Validation of the dynamic model with experimental results for varying FQ, N=1000 RPM, $T_{in} = 60^oC$, PR=20, SOI= 50 CAD bTDC

Thus we can conclude that the dynamic model is able to predict the experimental

CA50 and IMEP with reasonable accuracy. The next chapter centers on design of

RCCI combustion controllers.

Chapter 4

Linear Quadratic Integral (LQI) Control

In this chapter a model-based RCCI controller is developed to control combustion phasing (CA50) using Start of Injection (SOI) as the control variable. The dynamic model developed in Chapter 3 is used as a virtual plant model to initially test the designed controller. The controller is then validated by testing it on the experimental RCCI engine setup.

4.1 Simplified Control Oriented Model and Model Linearization

In Chapter 3 a dynamic model was developed to predict SOC, CA50 and BD. However the non-linear nature of the dynamic model makes it difficult to for use in the design of linear controllers. In this chapter the dynamic model is converted into simplified equations which will then be used to linearize the plant model. The linearized plant model is finally used to design an observer-based state-feedback controller for tracking CA50.

4.1.1 Simplified COM

The CA50 in RCCI combustion depends on parameters such as the air-fuel mixture temperature and pressure at intake valve closing, the fuel-air equivalence ratio (ϕ_{tot}), and the fuel premixed ratio (PR). Here, a linear empirical correlation is developed to estimate CA50. As shown in Equation (4.1) the coefficients of this correlation are

calculated by applying a linear regression fit to the experimental data.

$$CA50_k = C(1).PR_k + C(2).SOI_k + C(3).P_{ivc,k}$$

$$+ C(4).T_{ivc,k} + C(5).\phi_{tot,k} + C(6) \quad (4.1)$$

Where,

$$C = \begin{bmatrix} 0.2299 & -0.4041 & 0.6281 & -0.3435 & -0.1055 & 85.745 \end{bmatrix} \quad (4.2)$$

Figure 4.1 shows the simplified linear COM is able to predict the CA50 with reason-
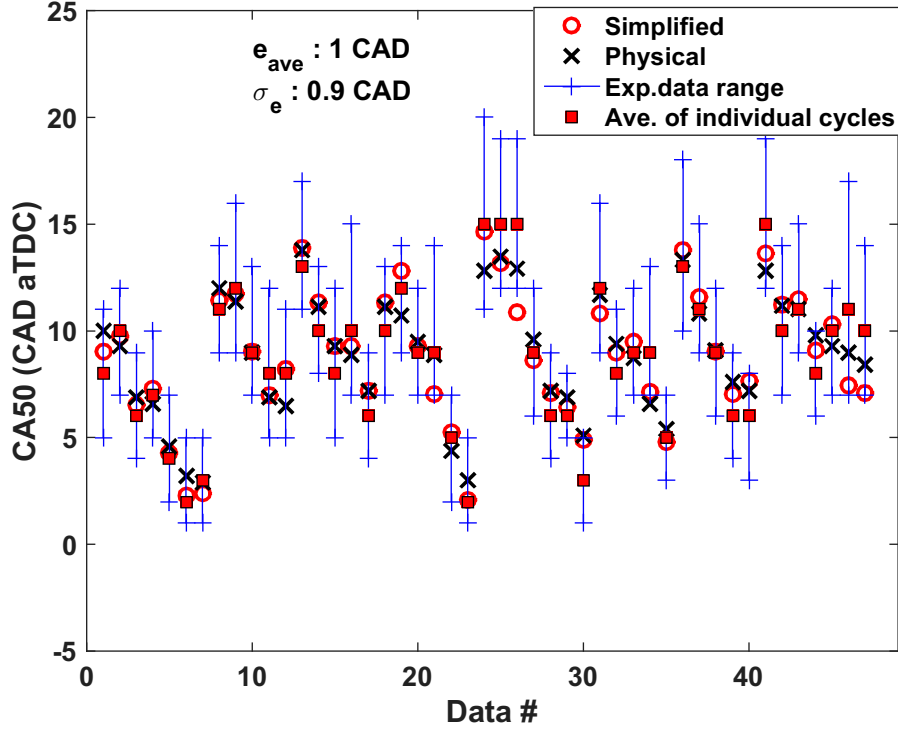
Figure 4.1: Validation of the simplified COM against experimental CA50 and predicted CA50 from the detailed physical model (Chapter3). e_{ave} and σ_e show the average and standard deviation of errors between CA50 from the simplified COM and the experimental CA50.

able accuracy for the experimental conditions studied. This empirical model is also
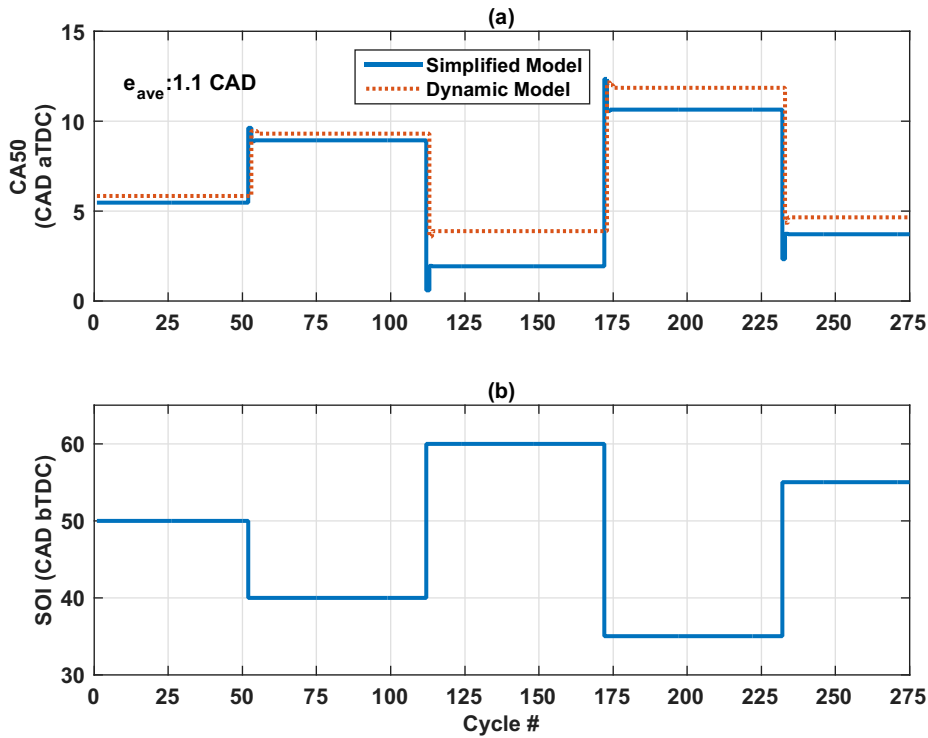
Figure 4.2: Validation of the simplified model against the dynamic RCCI model (Chapter3) for a step change in SOI at PR=20, FQ=23 mg/cycle and T_{in}=313.1 K.

validated against the detailed dynamic model for transient RCCI operations. Figure

4.2 shows the results of the two models.

4.1.2 State-Space RCCI Model

For designing a state-feedback controller we need to select states that completely

describe the RCCI engine operation. The following variables are selected as states of

the simplified COM:

56

1. Crank angle for 50% mass fraction burned (CA50)

2. Temperature at Start of Combustion (T_{soc})

3. Pressure at Start of Combustion (P_{soc})

4. Residual gas temperature (T_{rg})

By considering a cycle to start from IVC, the states of the current cycle $(k+1)$ can be expressed as a function of the states of the previous cycle (k) and inputs of the current cycle $(k+1)$ by including the cycle to cycle thermal coupling in the dynamic model.

$$CA50_{k+1} = f_1(CA50_k, T_{soc,k}, P_{soc,k}, T_{rg,k}, SOI_k, PR_k, FQ_{tot,k}) \qquad (4.3)$$

$$T_{soc,k+1} = f_2(CA50_k, T_{soc,k}, P_{soc,k}, T_{rg,k}, SOI_k, PR_k, FQ_{tot,k}) \qquad (4.4)$$

$$P_{soc,k+1} = f_3(CA50_k, T_{soc,k}, P_{soc,k}, T_{rg,k}, SOI_k, PR_k, FQ_{tot,k}) \qquad (4.5)$$

$$T_{rg,k+1} = f_4(CA50_k, T_{soc,k}, P_{soc,k}, T_{rg,k}, SOI_k, PR_k, FQ_{tot,k}) \qquad (4.6)$$

This can be expressed in the form of a state space equation:

$$X_{k+1} = A.X_k + B_i.u_k + B_d.w_k \qquad (4.7)$$

57

and

$$y_{k+1} = C.X_{k+1} + D.u_{k+1} \qquad (4.8)$$

where

$$X = \begin{bmatrix} CA50 & T_{soc} & P_{soc} & T_{rg} \end{bmatrix}^{T} \qquad (4.9)$$

$$u = \begin{bmatrix} SOI \end{bmatrix} \qquad (4.10)$$

$$w = \begin{bmatrix} PR \end{bmatrix} \qquad (4.11)$$

$$y = \begin{bmatrix} CA50 \end{bmatrix} \qquad (4.12)$$

Where X is the state vector, u is the vector of inputs, y is the output vector and w is the disturbance vector.

For LQI controller design, the simplified COM is linearlized around an operating point given in Table 4.1.

Table 4.1

Operating conditions of the linearization point for the design of an LQI controller

Parameter	Value
$CA50$ (CAD aTDC)	8
T_{soc} (K)	772.1
P_{soc} (kPa)	1828.47
T_{rg} (K)	863.9
FQ (mg/cycle)	23
SOI (CAD bTDC)	42.7
PR (-)	20
T_{in} (K)	333.1
P_{man} (kPa)	96.5

The plant matrices are as follows

$$A = \begin{bmatrix} -0.1658 & -0.01754 & 0.007405 & -0.009838 \\ 0.8424 & 0.08911 & -0.03763 & 0.04999 \\ -1.3 & -001375 & 0.05807 & -0.7715 \\ -0.6189 & -0.06546 & 0.02764 & -0.01133 \end{bmatrix} \tag{4.13}$$

$$B_i = \begin{bmatrix} -0.4165 & -0.3423 & -3.267 & -2.32 \end{bmatrix}^T \tag{4.14}$$

$$B_d = \begin{bmatrix} 0.2207 & -0.1814 & 1.731 & 1.204 \end{bmatrix}^T \tag{4.15}$$

$$C = \begin{bmatrix} 1 & 0 & 0 & 0 \end{bmatrix} \tag{4.16}$$

$$D = \begin{bmatrix} 0 \end{bmatrix} \tag{4.17}$$

4.2 Linear Quadratic Integral Control

A Linear Quadratic Integral (LQI) controller is designed to track the desired CA50 trajectory. An LQI controller is a full-state feedback optimal controller with a linear state function and a quadratic cost function [79]. Since the LQI is a model-based controller it can outperform a PID controller while controlling transient operation of a system, particularly against system disturbances [80]. A full-state feedback is required for LQI controller. If all the states are not measurable, then an observer/estimator is required, as will be designed in Section 4.2.2. For applying LQI control, a non-linear system needs to be linearized around a stable operating point (see Table 4.1). The performance of the controller deteriorates as the operating region moves away from the stable operating point. Another limitation of an LQI controller is that it cannot handle constraints as the control law is solely based on optimal cost computation. Figure 4.3 shows an overview of structure of the LQI controller designed for RCCI combustion phasing control.
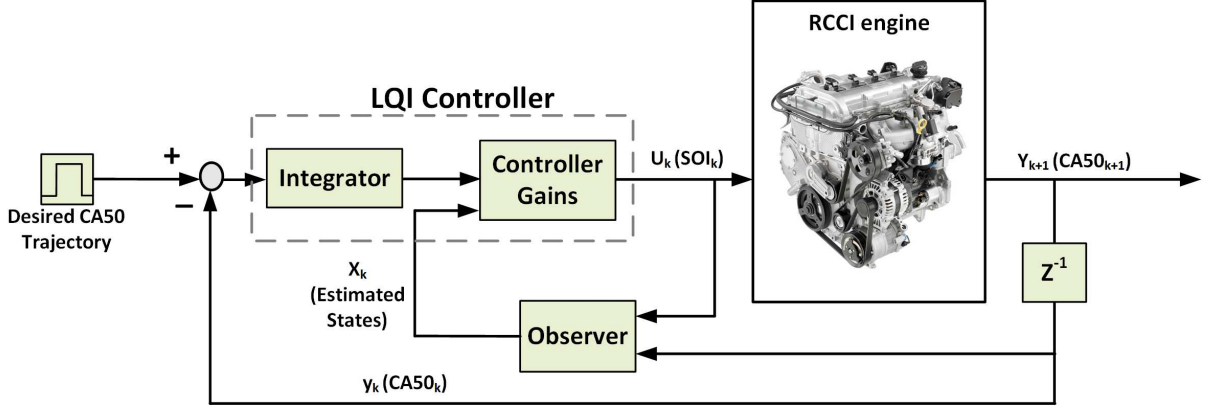
Figure 4.3: Structure of the designed RCCI combustion phasing controller

In order to include the integral state (X_i) into the plant model, the plant model is augmented by modifying state vector.

$$X_{aug,k} = \begin{bmatrix} X_k \\ X_i \end{bmatrix} \tag{4.18}$$

Therefore, the following augmented plant model is obtained:

$$X_{aug,k+1} = \begin{bmatrix} A & 0 \\ C & I \end{bmatrix} X_{aug,k} + \begin{bmatrix} B_i \\ 0 \end{bmatrix} u_k \tag{4.19}$$

4.2.1 Control law

An LQI controller minimizes the following cost function (J)

$$J = \frac{1}{2} \sum_{k=1}^{\infty} [X_{aug}^T(k) Q X_{aug}(k) + u^T(k) R\ u(k)] \tag{4.20}$$

where Q and R are semi-positive definite and positive definite matrix, respectively. The control law is given by:

$$u_k = -K.X_{aug,k} \tag{4.21}$$

K is the feedback gain given by

$$K = (R + B_{aug}^T P B_{aug})^{-1} B_{aug}^T P A_{aug} \tag{4.22}$$

where P is calculated by solving the discrete-time algebraic Riccati Equation (DARE): [81]:

$$P = A_{aug}^T P A - A_{aug}^T P B_{aug} (R + B_{aug}^T P B_{aug})^{-1} B_{aug}^T P A_{aug} + Q \tag{4.23}$$

4.2.2 State Estimator Design

The CA50 is the only measurable state of the system. In order to get full state feedback an observer is designed. The observer estimates the current states of the system (X_k) based on the current output measurement (y_k) and the system input (u_k). A Kalman Filter is designed as a state estimator. This also gives the added advantage of filtering out the measurement noise. The designed estimator is represented by Equation (4.24) and (4.25):

$$\hat{X}[k|k] = \hat{X}[k|k-1] + M(y_c[k] - C\hat{X}[k|k-1]) \tag{4.24}$$

$$\hat{X}[k+1|k] = A\hat{X}[k|k] + Bu[k] \tag{4.25}$$

where $\hat{X}$ is the estimated state vector and M is the observer gain. $\hat{X}[k+1|k]$ signifies the predicted value of $\hat{X}$ at engine cycle $k+1$ based on information available at cycle k. The gain M is calculated using Equation (4.26)

$$M = PC^T(CPC^T + \bar{R})^{-1} \tag{4.26}$$

Where, $\bar{Q}$ and $\bar{R}$ are the process noise and measurement noise covariance matrix respectively. An initial estimate of $\bar{R}$ is obtained by calculating the covariance of an open loop measurement. The initial value of $\bar{Q}$ is taken close to zero [82] and later

tuned for best performance. P is obtained by solving the DARE given by Equation (4.27). This calculation can be simplified by using the MATLAB® command *kalman* [83]

$$P = B_d \bar{Q} B_d^T + APA^T - APC^T(CPC^T + \bar{R})^{-1}CPA^T \quad (4.27)$$
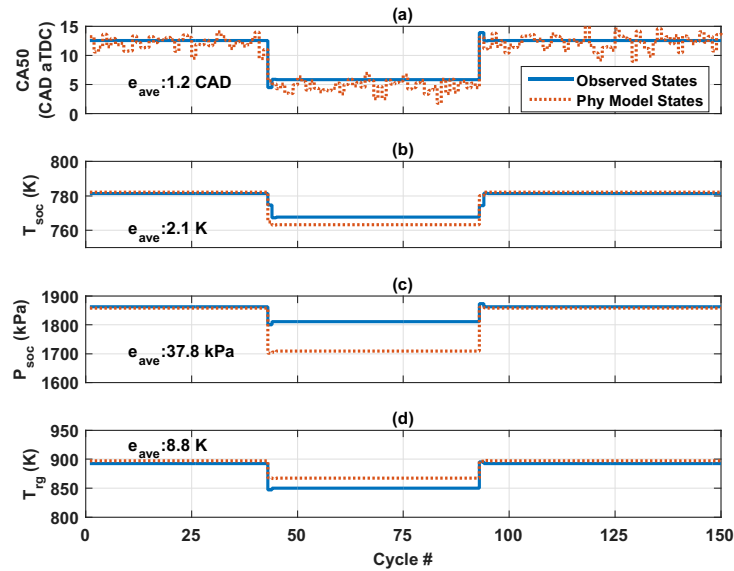
Figure 4.4: State-Observer Performance

In order to validate the state estimator, the estimated states are compared with the states of the dynamic model. Figure 4.4 shows the performance of the designed state estimator. A measurement noise of standard deviation of 1.1 CAD (based on experimental data) was added to the output of the dynamic model to test the estimator's response to noise. It can be seen that the estimator is able to filter out the noise while estimating the four required states. The estimator error is small

enough not to adversely affect the performance of the LQI controller. The errors between the states of the physical system and the observed states are due to model mismatch.

4.3   Simulation and Experimental Results

In this section, performance of the designed LQI controller is first evaluated on a virtual engine (detailed physical model from Chapter 3). Next, performance of the controller is tested on a real engine.

4.3.1   CA50 Tracking

Figures 4.5 and 4.6 show the simulation and experimental results of the LQI controller, respectively. The controller is able to track the reference CA50 without any steady state error in the simulation results. In the experimental results, due to measurement noise an average error of 1.6 CAD is observed.
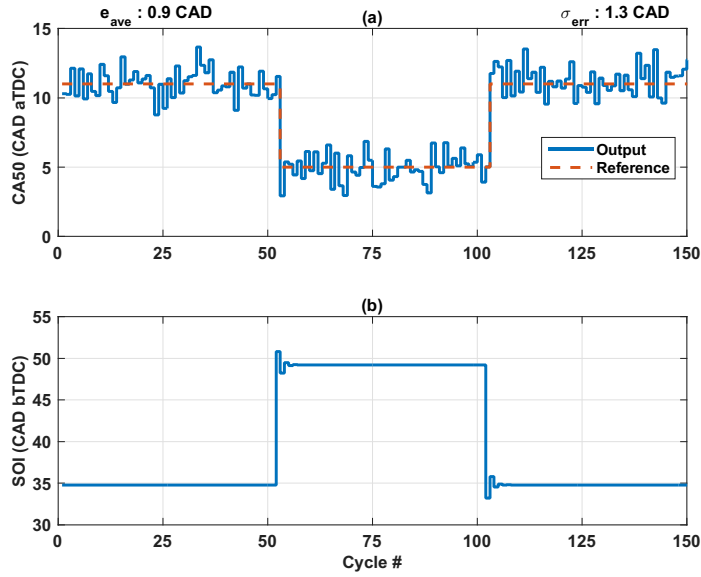
Figure 4.5: <u>Simulation</u> CA50 Tracking Results. Operating conditions: N= 1000 RPM, PR = 20, FQ= 23mg/cycle, T_{in}= 313.1K
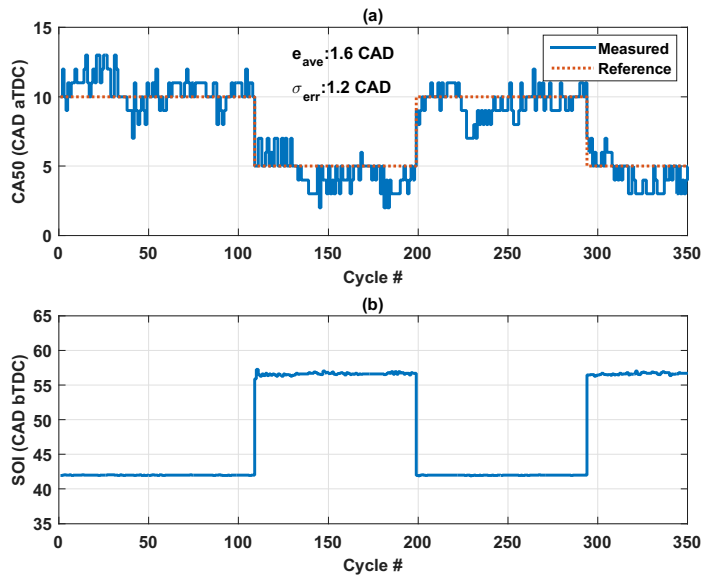
Figure 4.6: <u>Experimental</u> CA50 Tracking Results. Operating conditions: N= 1000 RPM, PR = 20, FQ= 23mg/cycle, T_{in}= 313.1 K

4.3.2 Disturbance Rejection

It is important that the designed controller can operate over a range of PR values.
PR variations are included in the controller design via a disturbance term. To test
the disturbance rejection capability of the controller a PR step of 20 was given. As
seen in Figure 4.7 the controller is able to track CA50 despite the sudden change in
PR.
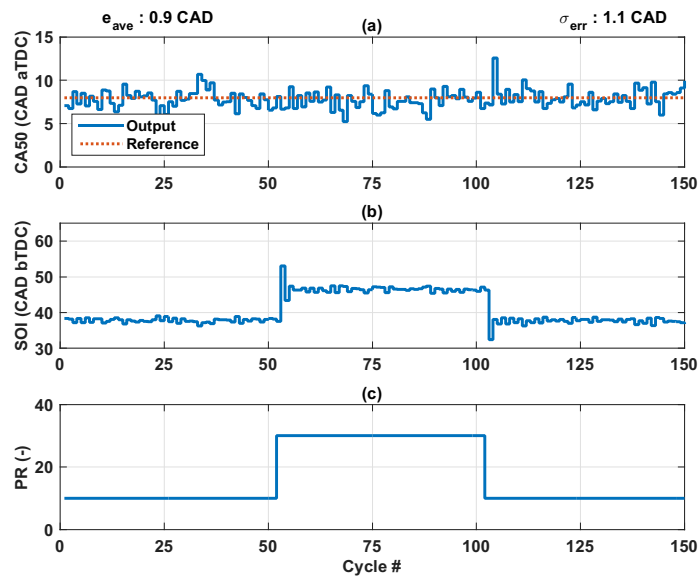
Figure 4.7: <u>Simulation</u> results for disturbance rejection when a PR step is given, FQ= 23 mg/cycle, T_{in}= 313.1 K, N= 1000 RPM at naturally aspirated conditions
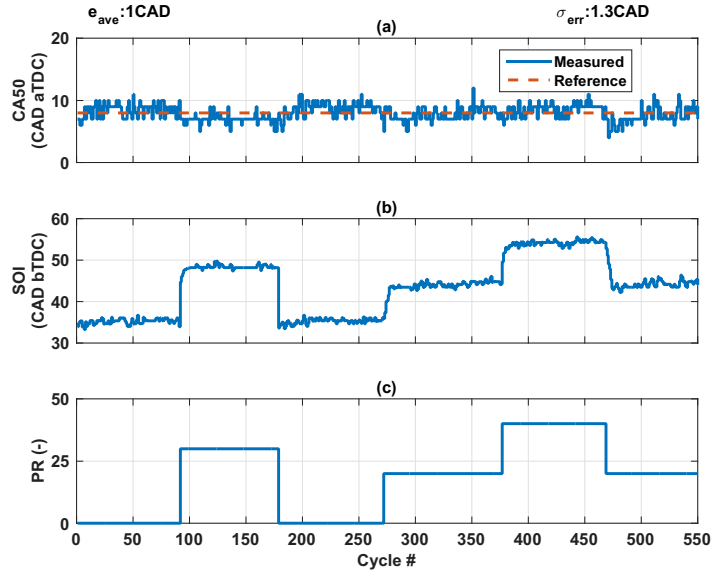
Figure 4.8: Experimental results for disturbance rejection when a PR step is given, FQ= 23 mg/cycle, $\overline{T_{in}}$= 313.1 K, N= 1000 RPM, At naturally aspirated conditions

Figure 4.8 shows the experimental disturbance rejection capability of the controller.

The PR is varied from 0 to 40 in multiple steps. The controller is able to track the

reference CA50 with an average error of 1 CAD.

Chapter 5

Model Predictive Control of

Combustion Phasing and Load

This chapter discusses the development of a MIMO COM and a model predictive controller (MPC) for controlling combustion phasing and engine load (IMEP) in the RCCI engine. Furthermore, a strategy to select between PR and SOI as control variables is also designed.

5.1 Development of MIMO COM and Model Linearization

As discussed previously in Chapter 4 a simplified COM for CA50 was developed. In order to fully define the plant model, the IMEP is added as a new state. To remove plant model complexity T_{rg} is removed from plant states. Thus the states of the MIMO COM are defined as:

1. Crank angle for 50% fuel mass fraction burned ($CA50$)

2. Temperature at Start of Combustion (T_{soc})

3. Pressure at Start of Combustion (P_{soc})

4. Indicated Mean Effective Pressure ($IMEP$)

These states are then expressed as a function of the states of the previous cycle and thus can be expressed in state space form as shown in Equation (5.1)

$$X_{k+1} = A.X_k + B.U_k \tag{5.1}$$

and

$$Y_{k+1} = C.X_{k+1} + D.U_{k+1} \tag{5.2}$$

where,

$$X = \begin{bmatrix} CA50 & T_{soc} & P_{soc} & IMEP \end{bmatrix}^T \tag{5.3}$$

$$U = \begin{bmatrix} SOI & FQ \end{bmatrix}^T \quad or \quad U = \begin{bmatrix} PR & FQ \end{bmatrix}^T \tag{5.4}$$

$$Y = \begin{bmatrix} CA50 & IMEP \end{bmatrix}^T \tag{5.5}$$

This state space plant model is linearized around a nominal operating point. The operating conditions of the linearization point are given in Table 5.1.

Table 5.1
Operating conditions for the point used to linearize the MIMO COM

Parameter	Value
$CA50$ (CAD aTDC)	8
T_{soc} (K)	777.7
P_{soc} (kPa)	1828.4
$IMEP$ (kPa)	620
FQ (mg/cycle)	22.89
SOI (CAD bTDC)	40.4
PR (-)	20
T_{in} (K)	333.1
P_{man} (kPa)	96.5

The linearization yields the following plant matrices:

$$
A = \begin{bmatrix}
-0.1193 & -0.01442 & 0.005329 & 0.007647 \\
0.6055 & 0.07319 & -0.02705 & -0.03881 \\
-0.9355 & -0.1131 & 0.04179 & 0.05997 \\
-0.7149 & -0.06431 & 0.03193 & -0.04349
\end{bmatrix}
\tag{5.6}
$$

$$
B = \begin{bmatrix}
-0.4165 & -0.3448 & -3.267 & 2.259 \\
-0.3176 & 1.871 & -2.491 & 28.39
\end{bmatrix}^T
\tag{5.7}
$$

$$
C = \begin{bmatrix}
1 & 0 & 0 & 0 \\
0 & 0 & 0 & 1
\end{bmatrix}
\quad
D = \begin{bmatrix}
0 & 0 \\
0 & 0
\end{bmatrix}
\tag{5.8}
$$

5.2   Model Predictive Controller (MPC) Design

A 5-step prediction MPC is developed to control CA50 and IMEP. Control of IMEP is done by using the total fuel quantity (FQ) as the control variable. On the other hand, CA50 control is achieved by adjusting either SOI or PR. A strategy developed by Arora [43] is used to determine whether SOI or PR should be used as the control variable. In this section, initially separate controllers with PR and SOI as control variables are developed, simulated and validated on the experimental setup. Then, a unified control strategy is developed for MIMO MPC for the RCCI engine.

5.2.1 Controller Design

One of the major advantages of MPC is the ability to include state constrains and control actuator constraints. in the controller formulation. MPC is based on real-time iterative optimization of a plant model [84]. The model is optimized over a finite number of time steps and a control strategy is decided based on the optimization results. This finite number of time steps is called prediction horizon. Only the first step of the optimization strategy is implemented at the current time step and the entire optimization process is repeated for the next time step. Since the prediction horizon keeps shifting forward in time, MPC is also known as receding horizon control.

MPC requires fore-knowledge of the reference input over the prediction horizon. Based on this fore-knowledge, the states of the system over the prediction horizon are calculated. Thus the predictive control output can be defined as [84]:

$$Y_k = F.X_k + \phi.U_k \tag{5.9}$$

where,

$$Y_k = \begin{bmatrix} y(k_i + 1|k_i) & y(k_i + 2|k_i) & y(k_i + 3|k_i) & y(k_i + 4|k_i) & y(k_i + 5|k_i) \end{bmatrix}^T \tag{5.10}$$

$$F = \begin{bmatrix} CA \\ CA^2 \\ CA^3 \\ CA^4 \\ CA^5 \end{bmatrix} ; \phi = \begin{bmatrix} CB & 0 & 0 & 0 & 0 \\ CAB & CB & 0 & 0 & 0 \\ CA^2B & CAB & CB & 0 & 0 \\ CA^3B & CA^2B & CAB & CB & 0 \\ CA^5 & CA^3B & CA^2B & CAB & CB \end{bmatrix} \tag{5.11}$$

$y(k_i + N|k_i)$ is defined as the $i + N^{th}$ step prediction at step i. We can define the cost function as follows

$$J = \sum_{i=1}^{N} [(\Psi_i - Y_i)^T Q (\Psi_i - Y_i) + U_i^T R U_i] \tag{5.12}$$

Where Ψ is the vector of the reference inputs over the prediction horizon and Q and R are weights on the reference tracking and the control variable, respectively. The optimal solution to this cost function is given by [84]:

$$U = (\Phi^T Q \Phi + R)^{-1} \Phi^T Q (\Psi - F X_k) \tag{5.13}$$

To prevent the control variable from being set to values outside the safe operation limits of the engine, we impose amplitude constraints onto the control variable. Thus the optimal solution is subject to constraints and hence it can be expressed as a quadratic programming problem in terms of U as

$$J = \frac{1}{2} U^T E U + U^T H \tag{5.14}$$

74

subject to the constraints

$$A_{cons}U \leqslant B_{cons} \tag{5.15}$$

where

$$E = (\Phi^T Q \Phi + R); \;\; H = \Phi^T Q(\Psi - F X_k) \tag{5.16}$$

and

$$A_{cons} = \begin{bmatrix} 1 & 0 & 0 & 0 & 0 \\ -1 & 0 & 0 & 0 & 0 \end{bmatrix}; \;\; B_{cons} = \begin{bmatrix} U_{max} - u(k_i - 1) \\ U_{min} + u(k_i - 1) \end{bmatrix} \tag{5.17}$$

5.2.2 Tracking Performance

Figure 5.1 shows the simulation results for a MIMO MPC with PR and FQ as the control variables. The results show that the controller is able to track both CA50 and IMEP satisfactorily. A measurement noise is added to the output of CA50 and IMEP to test the controller response to experimental noise. In the experimental results shown in Figure 5.2 a simultaneous step of CA50 and IMEP is given. Due to cyclic variability and measurement noise we get an average tracking error of 1.1 CAD in CA50 and an error of 23.6 kPa in the IMEP results.

Figure 5.3 shows the simulation results for a MIMO MPC with SOI and FQ as the control variables. The results show that the controller is able to track both CA50 and IMEP satisfactorily when a simultaneous step is given to both CA50 and IMEP.
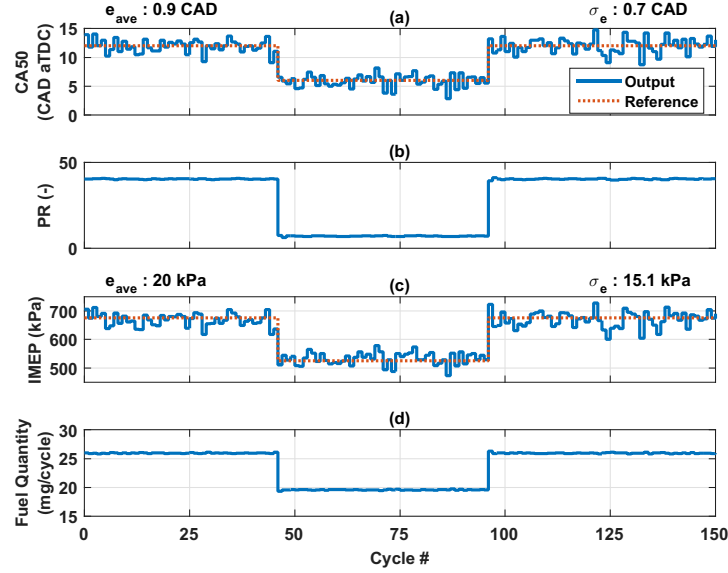
Figure 5.1: <u>Simulation</u> results for CA50 and IMEP control using PR and FQ as control variables. Operating conditions: SOI= 45 CAD bTDC, T_{in}= 333.1 K at 1000 RPM.
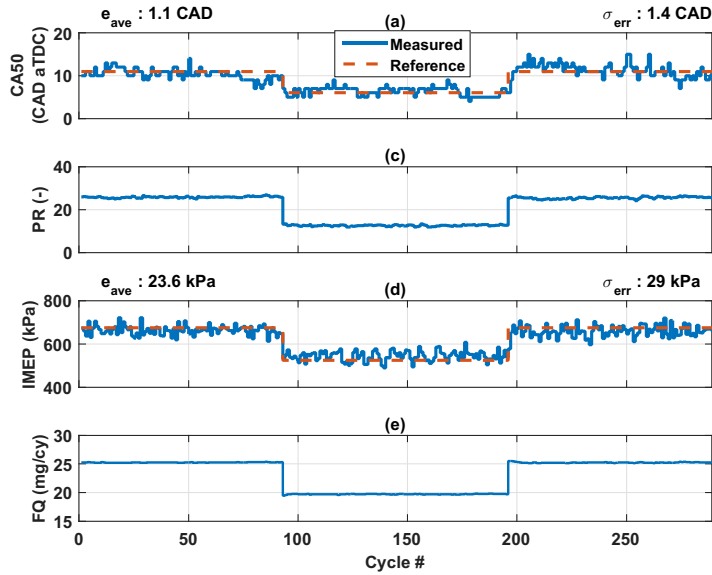
Figure 5.2: <u>Experimental</u> results for CA50 and IMEP control using PR and FQ as control variables. Operating conditions: SOI= 45 CAD bTDC, T_{in}= 333.1 K at 1000 RPM.

Figure 5.4 shows the experimental results for MIMO MPC with SOI and FQ as the control variables. Due to cyclic variability and measurement noise we get an average tracking error of 0.9 CAD in CA50 and an average error of 26.2 kPa in the IMEP

76

tracking results.
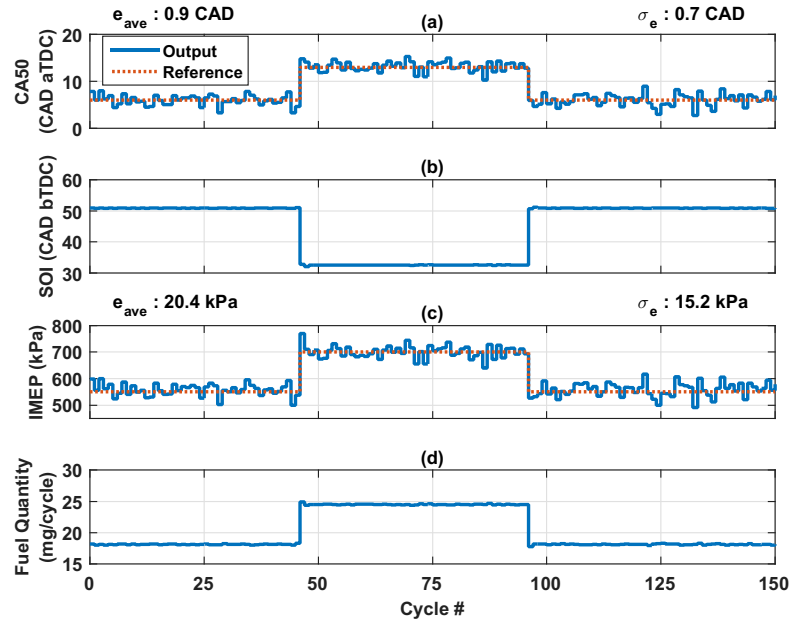
Figure 5.3: <u>Simulation</u> results for CA50 and IMEP control using SOI and FQ as control variables. Operating conditions: PR= 20, T_{in}= 333.1 K at 1000 RPM.
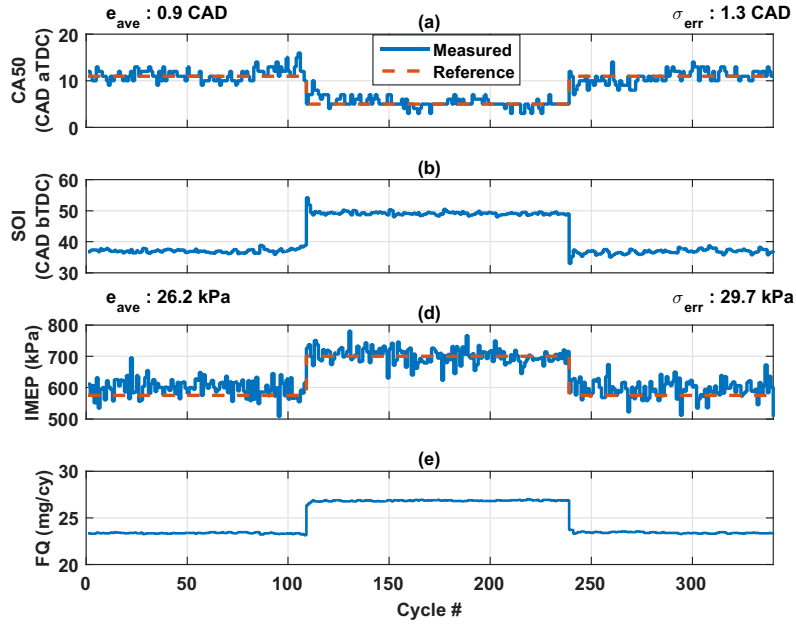
Figure 5.4: Experimental results for CA50 and IMEP control using SOI and FQ as control variables. Operating conditions: PR= 20, T_{in}= 333.1 K at 1000 RPM.

5.3 Switched MPC controllers

In Section 5.2.2, a MIMO MPC with SOI as the control variable was discussed. However this single MPC is only able to track the reference input in a small region around the nominal operating point. If we change operating region by changing parameters such as engine RPM, intake temperature or PR the controller performance degrades drastically. Figure 5.5 shows the effect of changing the operating region by
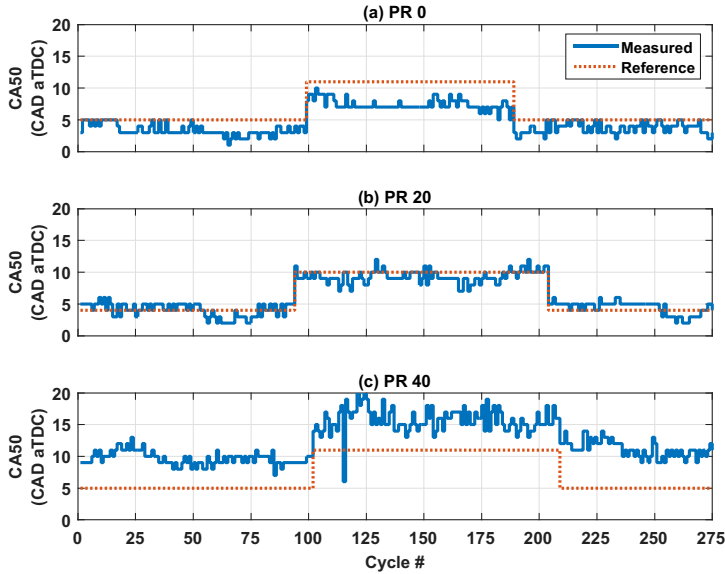
Figure 5.5: <u>Experimental</u> results of a SISO MPC at varying PR values, T_{in}=333.1 K at 1000 RPM

changing the PR on a single MPC. The MPC has been designed at PR20 and it is not able to track the CA50 when the PR is changed to 0 or 40. To increase the operating range of the controller, multiple MPCs can be designed. A scheduling parameter is selected which acts as a switch between multiple MPC controllers when the operating

region changes.

Thus a set of MPCs is designed with PR as the scheduling variable. Table 5.2 gives the operating range of each MPC.

Table 5.2
Operating range of individual controllers in switched MPC setup.

Controller Name	PR range
MPC_1	$5 < PR < 15$
MPC_2	$16 < PR < 25$
MPC_3	$26 < PR < 35$
MPC_4	$36 < PR < 45$

Figure 5.6 shows the experimental results of using switched MPCs with PR as the scheduling variable. The CA50 and IMEP are kept constant at 9 CAD aTDC and 600 kPa, respectively, while multiple step inputs are given on the PR. The controller is able to track the reference CA50 and IMEP over a wide range of PR ranging from 5 to 45. For instance when the PR is changed from 12 to 40 (between cycles 250 and 300), the operating region changes and control switches from MPC_1 to MPC_4. Due to cyclic variability and measurement noise, there is an average error of 1.3 CAD in CA50 and 23.8 kPa in IMEP tracking.
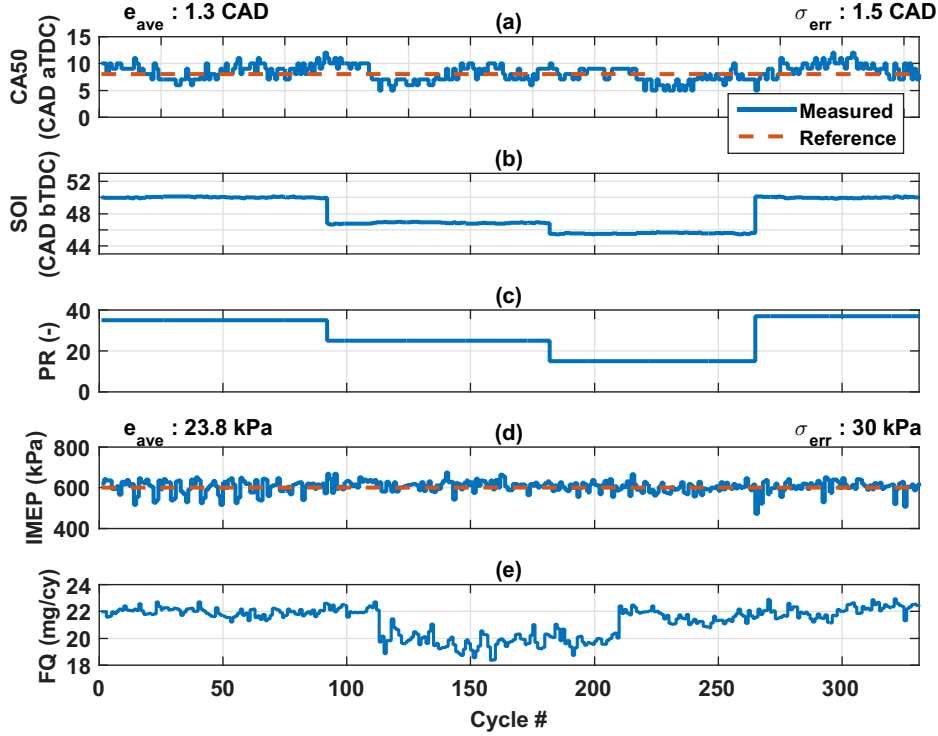
Figure 5.6: <u>Experimental</u> results for maintaining optimum CA50 and desired IMEP by using switched <u>MPCs</u> using PR as a scheduling variable, T_{in}=333.1 K at 1000 RPM

5.4   Sensitivity Based Controller Design

To decide whether PR or SOI should be used as the variable for CA50 control, a PR sweep for different values of SOI is conducted at constant engine speeds and intake conditions. The results of this sweep can be seen in Figure 5.7. We can observe from Figure 5.7, in the region marked with R1, CA50 is more sensitive to changes in PR and using PR as the control variable will result in a more effective way to control CA50, compared to using SOI. Similarly in the region marked with R2, the CA50 is more sensitive o changes in the SOI and using SOI as a control variable will be more

effective than PR. Thus a sensitivity factor is defined in Equation (5.18) which is used to select between PR or SOI control. If $S_{SOI} > S_{PR}$ then $S_{SOI}^{CA50} = 1$ and $S_{PR}^{CA50} = 0$; thus, SOI will be selected as the control variable and vice versa.
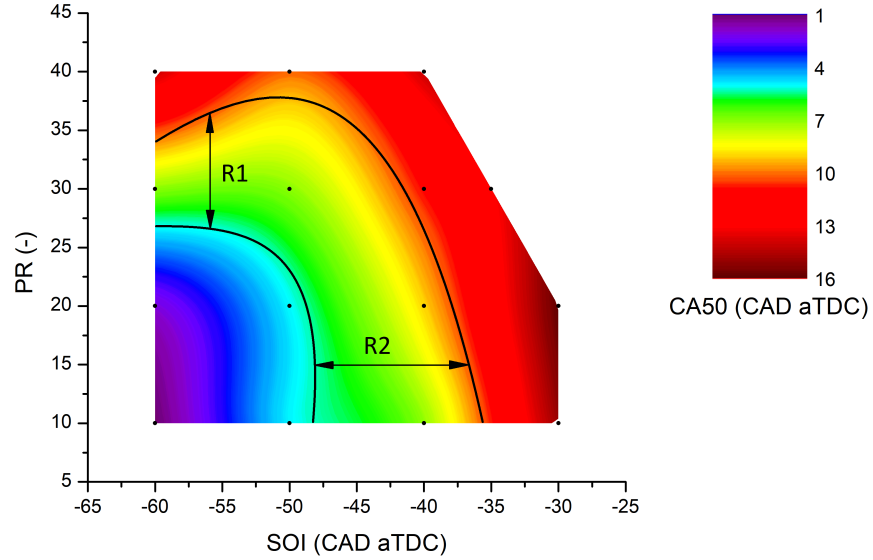
Figure 5.7: SOI and PR sweeps at $T_{in} = 60°C$ at 1000 RPM at naturally aspirated conditions. Experimental data points are shown by dot symbols.

$$S_{SOI} = \frac{dCA50}{dSOI} \frac{SOI}{CA50} \tag{5.18}$$

$$S_{PR} = \frac{dCA50}{dPR} \frac{PR}{CA50} \tag{5.19}$$
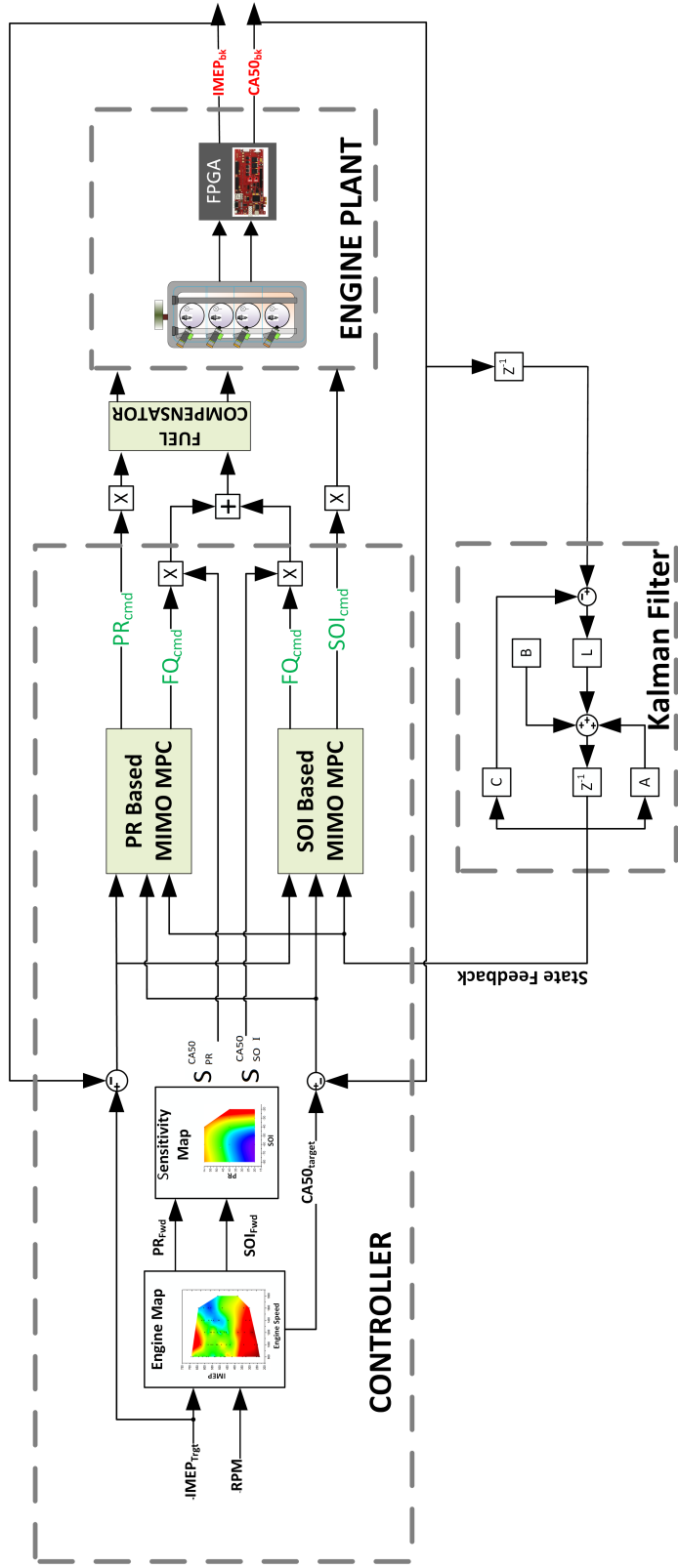
Figure 5.8: Schematic of the designed sensitivity based switched MPC controller for adjusting RCCI combustion phasing (CA50) and load (IMEP)

The entire controller structure can be summarized as shown in Figure 5.8. The maximum thermal efficiency, maximum allowable pressure rise rate, allowable peak in-cylinder pressure, and combustion stability (COV_{IMEP}) were all considered while making the engine map which is part of the designed controller structure. Based on the current load and speed requirements, the engine map will provide feed-forward values of PR, SOI and CA50. Based on the sensitivity values, either SOI or PR control will be utilized. Next, switched MPC controllers will adjust CA50 and IMEP to desired values. In addition, a feed-forward fuel compensator was included in the control structure to account for the lag caused by fuel dynamics through PFI injections. The transfer fucntion of the compensator was chosen as the inverse of the fuel dynamics model ($x - \tau_f$) developed in Section 3.6 [85].

$$G(s) = \frac{1 + \tau_f(1 - x)s}{1 + \tau_f s} \tag{5.20}$$

This compensator affects only transient response of the system.

5.4.1 Tracking Performance

First, the controller shown in Figure 5.8 is tested on the dynamic model from Chapter 3. A load step is given while the CA50 is held constant at 8 CAD aTDC. Measurement noise is added to the dynamic model to test the effect of noise on the controller.
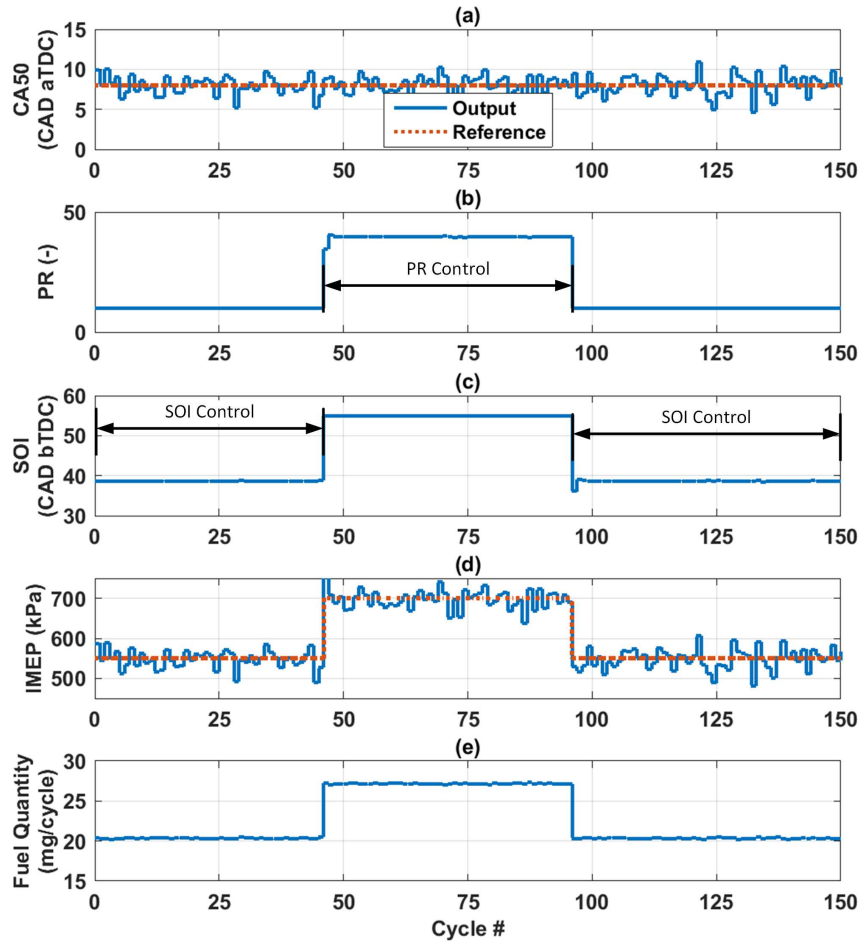
Figure 5.9: <u>Simulation</u> tracking results of the designed sensitivity based MPC, T_{in}= 333.1 K at 1000 RPM

Figure 5.9 shows that the controller is able to track CA50 and IMEP closely. At low load the CA50 is more sensitive to SOI hence the SOI based MPC is active. At the high load conditions, the PR controls gets activated. The controller is tested on the experimental setup with constant engine speed, intake temperature and pressure. The results are shown in Figure 5.10. The controller is able to track the combustion phasing and load closely with an average tracking error of 1.2 CAD in CA50 and 15.5
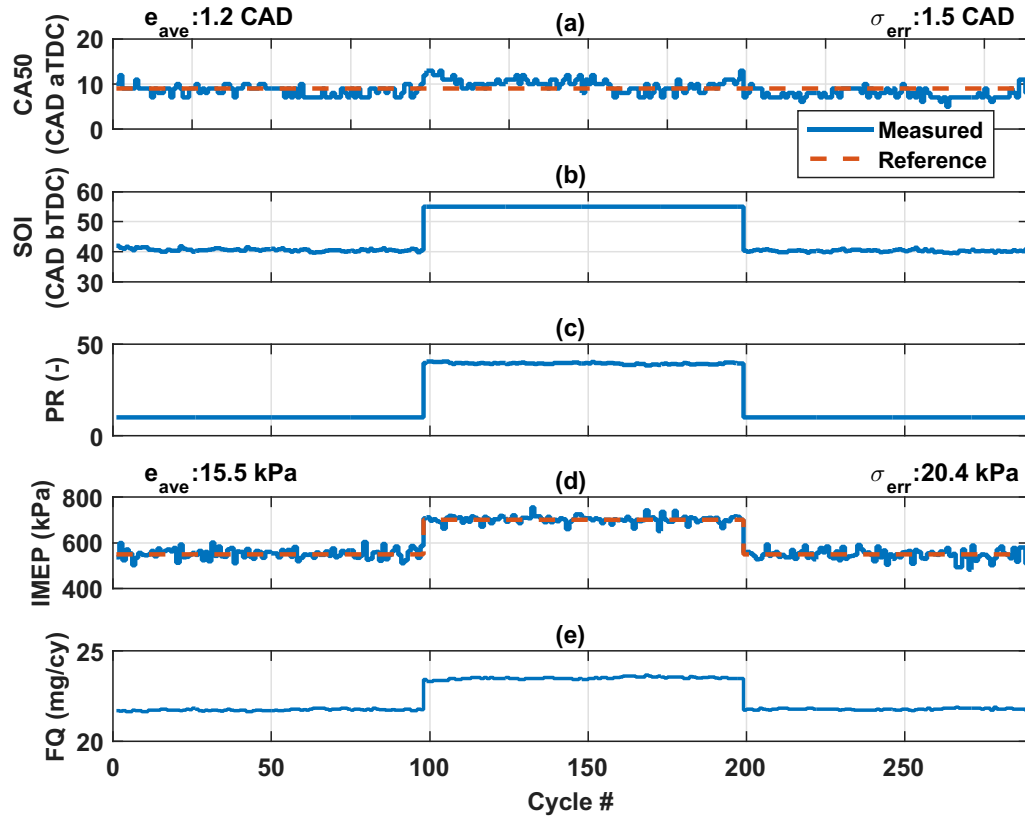
Figure 5.10: Experimental tracking results of the designed sensitivity based switched MPC, T_{in}=313.1 K at 1000 RPM

kPa in IMEP.

Chapter 6

Conclusions and Future Work

6.1   Conclusions

An experimental and simulation study was conducted to design optimal model-based RCCI engine controllers. Major contributions/findings from this thesis are summarized in the following:

  † Mean Value Models were developed for predicting CA50 and SOC. The Modified Knock Integral Model (MKIM) is able predict SOC with an average error of 1.9 CAD. The new modified Weibe model is able to predict the CA50 with an average error of 1 CAD.

† A physics based dynamic RCCI model was developed by incorporating the MVMs to predict CA50 and SOC along with other physics based equations. Cycle-to-cycle residual gas thermal coupling was modeled and a new model was developed to estimate IMEP. The dynamic RCCI model was then validated for transient operations including PR, SOI and FQ step changes. The experimental validation results show that the developed model can predict cycle-to-cycle CA50 and IMEP with average errors of 2.6 CAD and 43 kPa, respectively.

† The dynamic model was simplified and converted into state space form, Next, a single input single output Linear Quadratic Integral controller was developed. The LQI controller used SOI as the control input to control CA50 and had disturbance rejection capability to enable the the controller operation over a range of PR. A state observer was designed to estimate the non-measurable states of the system. The controller was tested out on the RCCi engine experimental setup. The controller was able to track the desired CA50 with an average error of 1.6 CAD. The controller was also able to reject the disturbance input PR and maintain the desired CA50.

† A multi input multi output MPC with a 5-cycle prediction horizon was developed to control both CA50 and IMEP. The MPC was tested out initially on the dynamic model using PR as the control input and then using SOI as the control input. The controller was then tested out on the experimental RCCI engine. The average errors for tracking CA50 and IMEP were found to be 1.1

CAD and 23.6 kPa when PR was used as the control input and 0.9 CAD and 26.2 kPa when SOI was used as the control input.

† The designed MPC could only work in a small operating region around the nominal operating point; thus switched MPC controllers were designed for different operating regions. PR was selected as the scheduling variable for switching between the MPC controllers. The experimental results showed that the controller is successfully able to maintain the desired CA50 and reach the required IMEP when the operating region changes.

† A sensitivity-based control strategy was developed in order to select between PR and SOI as the control variable to adjust CA50. An engine map was developed to decide the optimal operating point. Based on the sensitivity of CA50 at that operating point, a selection between PR or SOI control was made. Experimental results of the sensitivity based controller showed that the controller was able to track CA50 and IMEP over a wide RCCI operating range.

6.2   Future Work

Building upon the findings from this thesis, the following research avenues can be investigated to further improve the outcomes from this thesis:

† Since the dynamic model is non-linear, a non linear model based controller could be used to get better tracking results, though computational cost needs to be taken into account. Adaptive MPC controllers could be designed by using online model estimation or by developing Linear parametric varying (LPV) models for the RCCI engine.

† By incorporating exhaust gas thermofluid dynamics, the MPC could be extended to control exhaust gas temperature. This could be useful for maintaining the light-off temperatures of catalytic converters used for oxidizing tailpipe UHC and CO emissions.

† The MPC controller can be extended to control COV of IMEP. This can lead to a wider operating range of RCCI combustion. By controlling CA50 during transient operation while switching combustion modes, it is possible to extend the operating range even further.

† Increasing the compression ratio could lead to a wider operating range of the RCCI engine. This can be done by the newly designed pistons [46] for the engine.

† The RCCI controllers could be extended to include all the four engine cylinders in order to minimize cylinder-to-cylinder variability.

Bibliography

[1] U.S. Energy Information Administration. "Annual Energy Outlook with projections to 2050". `https://www.eia.gov/outlooks/aeo/`, 2017. Accessed on 06-24-2017.

[2] Office of Transportation and United States Environmental Protction Agency Air Quality. "EPA and NHTSA Set Standards to Reduce Greenhouse Gases and Improve Fuel Economy for Model Years 2017-2025 Cars and Light Trucks". 2012. EPA-420-F-12-051.

[3] Office of Transportation and Air Quality U.S. Environmental Protection Agency. "Draft Technical Assessment Report: Midterm Evaluation of Light-Duty Vehicle Greenhouse Gas Emission Standards and Corporate Average Fuel Economy Standards for Model Years 2022-2025". `https://www.nhtsa.gov/sites/nhtsa.dot.gov/files/draft-tar-final.pdf`, 2016. Accessed on 06-24-2017.

[4] J. B. Heywood. *"Internal combustion engine fundamentals",Chapter-11.*

Mcgraw-hill New York, 1988.

[5] T. Johnson. "Diesel emission control: 2001 in Review". SAE Technical Paper 2002-01-0285, 2002.

[6] D. Foster. "Low Temperature Combustion- A Thermodynamic Pathway to High Efficiency Engines". National Petroleum Council Fuels Study, published March 2012.

[7] D. Splitter, R. Hanson, S. Kokjohn, and R. Reitz. "Improving engine performance by optimizing fuel reactivity with a dual fuel PCCI strategy". *Conference on Thermo and Fluid Dynamic Processes in Diesel Engines*, 2010. Valencia, Spain.

[8] R. Hasegawa and H. Yanagihara. "HCCI combustion in DI diesel engine". 2003. SAE Technical Paper 2003-01-0745.

[9] G. Shibata, K. Oyama, T. Urushihara, and T. Nakano. "Correlation of Low Temperature Heat Release With Fuel Composition and HCCI Engine Combustion". 2005. SAE Technical Paper 2005-01-0138.

[10] R. Opat, Y. Ra, M. Gonzalez, R. Krieger, R. Reitz, and D. et al Foster. "Investigation of mixing and temperature effects on HC/CO emissions for highly dilute low temperature combustion in a light duty diesel engine". 2007. SAE Technical Paper 2007-01-0193.

[11] S. Kokjohn, R. Hanson, D. Splitter, and R. Reitz. "Experiments and modeling

of dual-fuel HCCI and PCCI combustion using in-cylinder fuel blending". *SAE International Journal of Engines*, 2(2):24–39, 2009.

[12] K. Inagaki, T. Fuyuto, K. Nishikawa, K. Nakakita, and I. Sakata. "Dual-fuel PCI combustion controlled by in-cylinder stratification of ignitability". SAE Technical Paper 2006-01-0028, 2006.

[13] S. Kokjohn, R. Hanson, D. Splitter, and R. Reitz. "Fuel reactivity controlled compression ignition (RCCI): a pathway to controlled high-efficiency clean combustion". *International Journal of Engine Research*, 12(3):209–226, 2011.

[14] A. Paykani, A. Kakaee, P. Rahnama, and R. Reitz. "Progress and recent trends in reactivity-controlled compression ignition engines". *International Journal of Engine Research*, 17(5):481–524, 2016.

[15] S. Kokjohn and R. Reitz. "Reactivity controlled compression ignition and conventional diesel combustion: A comparison of methods to meet light-duty NOx and fuel economy targets". *International Journal of Engine Research*, 14(5):452–468, 2013.

[16] S. Curran, R. Hanson, R. Wagner, and R. Reitz. "Efficiency and emissions mapping of RCCI in a light-duty diesel engine". 2013. SAE Technical Paper 2013-01-0289.

[17] D. Klos and S. Kokjohn. "Investigation of the effect of injection and control strategies on combustion instability in reactivity-controlled compression ignition

engines". *Journal of Engineering for Gas Turbines and Power*, 138(1):011502, 2016.

[18] D. Splitter, R. Hanson, S. Kokjohn, M. Wissink, and R. Reitz. "Injection effects in low load RCCI dual-fuel combustion". 2011. SAE Technical Paper 2011-24-0047.

[19] P. Zoldak, A. Sobiesiak, M. Bergin, and D. Wickman. "Computational study of reactivity controlled compression ignition (RCCI) combustion in a heavy-duty diesel engine using natural gas". 2014. SAE Technical Paper 2014-01-1321.

[20] D. Nieman, A. Dempsey, and R. Reitz. "Heavy-duty RCCI operation using natural gas and diesel". *SAE International Journal of Engines*, 5(2012-01-0379):270–285, 2012.

[21] Y. Li, M. Jia, Y. Chang, Y. Liu, M. Xie, T. Wang, and L. Zhou. "Parametric study and optimization of a RCCI (reactivity controlled compression ignition) engine fueled with methanol and diesel". *Energy*, 65:319–332, 2014.

[22] V. Soloiu et al. "Simultaneous Reduction of NO X and Soot in a Diesel Engine through RCCI Operation with PFI of n-butanol and DI of Cottonseed Biodiesel". 2014. SAE Technical Paper 2014-01-1322.

[23] J. Lim and R. Reitz. "Improving the efficiency of low temperature combustion engines using a chamfered ring-land". *Journal of Engineering for Gas Turbines and Power*, 137(11):111509, 2015.

[24] D. Splitter, M. Wissink, S. Kokjohn, and R. Reitz. "Effect of compression ratio and piston geometry on RCCI load limits and efficiency". 2012. SAE Technical Paper 2012-01-0383.

[25] A. Dempsey, N. Walker, and R. Reitz. "Effect of cetane improvers on gasoline, ethanol, and methanol reactivity and the implications for RCCI combustion". *SAE International Journal of Fuels and Lubricants*, 6(1):170–187, 2013.

[26] H. Wang, D. DelVescovo, M. Yao, and R. Reitz. "Numerical study of RCCI and HCCI combustion processes using gasoline, diesel, iso-butanol and DTBP cetane improver". *SAE International Journal of Engines*, 8(2):831–845, 2015.

[27] M. Wissink. *"Direct injection for dual fuel stratification (DDFS): Improving the control of heat release in advanced IC engine combustion strategies"*. PhD thesis, University Of Wisconsin-Madison, 2015.

[28] S. Kokjohn, R. Hanson, D. Splitter, J. Kaddatz, and R. Reitz. "Fuel reactivity controlled compression ignition (RCCI) combustion in light-and heavy-duty engines". *SAE International Journal of Engines*, 4(1):360–374, 2011.

[29] D. Splitter, R. Reitz, and R. Hanson. "High efficiency, low emissions RCCI combustion by use of a fuel additive". *SAE International Journal of Fuels and Lubricants*, 3(2):742–756, 2010.

[30] J. Benajes, S. Molina, A. García, E. Belarte, and M. Vanvolsem. "An investigation on RCCI combustion in a heavy duty diesel engine using in-cylinder blending of diesel and gasoline fuels". *Applied Thermal Engineering*, 63(1):66–76, 2014.

[31] M. Wissink, J. Lim, D. Splitter, R. Hanson, and R. Reitz. "Investigation of injection strategies to improve high efficiency RCCI combustion with diesel and gasoline direct injection". In *ASME 2012 Internal Combustion Engine Division Fall Technical Conference*, pages 327–338. American Society of Mechanical Engineers, 2012.

[32] S. Kokjohn, R. Reitz, D. Splitter, and M. Musculus. "Investigation of fuel reactivity stratification for controlling PCI heat-release rates using high-speed chemiluminescence imaging and fuel tracer fluorescence". *SAE International Journal of Engines*, 5(2):248–269, 2012.

[33] D. Splitter, M. Wissink, D. DelVescovo, and R. Reitz. "RCCI engine operation towards 60% thermal efficiency". 2013. SAE Technical Paper 2013-01-0279.

[34] P Brijesh, A Chowdhury, and S Sreedhara. "Advanced combustion methods for simultaneous reduction of emissions and fuel consumption of compression ignition engines". *Clean Technologies and Environmental Policy*, 17(3):615, 2015.

[35] D. Splitter, S. Kokjohn, K. Rein, R. Hanson, S. Sanders, and R. Reitz. "An optical investigation of ignition processes in fuel reactivity controlled PCCI combustion". *SAE International Journal of Engines*, 3(2010-01-0345):142–162, 2010.

[36] D. Zhou, W. Yang, H. An, and J. Li. "Application of CFD-chemical kinetics approach in detecting RCCI engine knocking fuelled with biodiesel/methanol". *Applied Energy*, 145:255–264, 2015.

[37] A. Dempsey, S. Curran, and R. Reitz. "Characterization of reactivity controlled compression ignition (RCCI) using premixed gasoline and direct-injected gasoline with a cetane improver on a multi-cylinder engine". *SAE International Journal of Engines*, 8(2015-01-0855):859–877, 2015.

[38] N. Kondipati. "Experimental Study, Modelling and Controller Design for an RCCI Engine". Master's thesis, Michigan Technological University, 2016.

[39] Y. Wu, R. Hanson, and R. Reitz. "Investigation of Combustion Phasing Control Strategy During Reactivity Controlled Compression Ignition (RCCI) Multicylinder Engine Load Transitions". *Journal of Engineering for Gas Turbines and Power*, 136(9):091511, 2014.

[40] C. Bekdemir, R. Baert, F. Willems, and B. Somers. "Towards control-oriented modeling of natural gas-diesel RCCI combustion". 2015. SAE Technical Paper 2015-01-1745.

[41] A. Indrajuana, C. Bekdemir, X. Luo, and F. Willems. "Robust multivariable feedback control of natural gas-diesel RCCI combustion". *IFAC-PapersOnLine*, 49(11):217–222, 2016.

[42] K.K. Sadabadi. "Modelling and Control of Combustion Phasing of an RCCI Engine". Master's thesis, Michigan Technological University, 2015.

[43] J. Arora and M. Shahbakhti. "Real-Time Closed-Loop Control of a Light-Duty RCCI Engine During Transient Operations". 2017. SAE Technical Paper 2017-01-0767.

[44] J. Arora. "Design of real-time combustion feedback system and experimental study of an RCCI engine for control". Master's thesis, Michigan Technological University, 2016.

[45] D. Kothari. "Experimental Setup and Design for an RCCI Engine". Master's thesis, Michigan Technological University, 2014.

[46] H. Saigaonkar. "An Investigation of variable valve timing effects on HCCI Engine Performance". Master's thesis, Michigan Technological University, 2014.

[47] K. Kannan. "An Experimental investigation of Low Temperature Combustion (LTC) regimes in a light duty engine". Master's thesis, Michigan Technological University, 2016.

[48] K. Owen and T. Coley. *"Automotive fuels reference book"*. Society of Automotive Engineers, Warrendale, PA (United States), 1995.

[49] B. Taylor and C. Kuyatt. *"Guidelines for evaluating and expressing the uncertainty of NIST measurement results"*. US Department of Commerce, Technology

Administration, National Institute of Standards and Technology Gaithersburg, MD, 1994.

[50] S. Kokjohn. *"Reactivity controlled compression ignition (RCCI) combustion"*. PhD thesis, University Of Wisconsin-Madison, 2012.

[51] A. Kakaee, P. Rahnama, and A. Paykani. "Numerical study of reactivity controlled compression ignition (RCCI) combustion in a heavy-duty diesel engine using 3D-CFD coupled with chemical kinetics". *International Journal of Automotive Engineering*, 4(3):792–804, 2014.

[52] M. Shahbakhti. *"Modeling and experimental study of an HCCI engine for combustion timing control"*. PhD thesis, University of Alberta, 2009.

[53] M. Bidarvatan. *"Physics-based modeling and control of powertrain systems integrated with Low Temperature Combustion engines"*. PhD thesis, Michigan Technological University, 2015.

[54] G. Shaver, J Christian Gerdes, Matthew J Roelle, Patrick A Caton, and Christopher F Edwards. "Dynamic modeling of residual-affected homogeneous charge compression ignition engines with variable valve actuation". *Journal of Dynamic Systems, Measurement, and Control*, 127(3):374–381, 2005.

[55] A. Vandersickel, M. Hartmann, K. Vogel, Y. Wright, M. Fikri, R. Starke, C. Schulz, and K. Boulouchos. "The autoignition of practical fuels at HCCI

conditions: High-pressure shock tube experiments and phenomenological modeling". *Fuel*, 93:492–501, 2012.

[56] L. Pickett, D. Siebers, and C. Idicheria. "Relationship between ignition processes and the lift-off length of diesel fuel jets". 2005. SAE Technical Paper 2005-10-24.

[57] S. Kook, C. Bae, P. Miles, D. Choi, and L. Pickett. "The influence of charge dilution and injection timing on low-temperature diesel combustion and emissions". 2005. SAE Technical Paper 2005-10-24.

[58] M. Andersson, B. Johansson, A. Hultqvist, and C. Noehre. "A predictive real time NOx model for conventional and partially premixed diesel combustion". 2006. SAE Technical Paper 2006-01-3329.

[59] S. Loganathan, R. Manohar, R. Thamaraikannan, R. Dhanasekaran, A. Rameshbabu, and V. Krishnamoorthy. "Direct injection diesel engine rate of heat release prediction using universal load correction factor in double wiebe function for performance simulation". 2012. SAE Technical Paper 2011-01-2456.

[60] D. Kim, M. Kim, and C. Lee. "Effect of premixed gasoline fuel on the combustion characteristics of compression ignition engine". *Energy & Fuels*, 18(4):1213–1219, 2004.

[61] G. Shaver, J. Gerdes, P. Jain, P. Caton, and C. Edwards. "Modeling for control of HCCI engines". 1:749–754, 2003.

[62] J. Bengtsson, M. Gafvert, and P. Strandh. "Modeling of HCCI engine combustion for control analysis". 2:1682–1687, 2004.

[63] Y. Kobashi, K. Fujimori, H. Maekawa, S. Kato, D.e Kawano, and J. Senda. "Modeling of auto-ignition and combustion processes for dual-component fuel spray". *SAE International Journal of Engines*, 4(2011-24-0001):2193–2206, 2011.

[64] Y. Suzuki, J. Kusaka, M. Ogawa, H. Ogai, S. Nakayama, and T. Fukuma. "Modeling of Diesel Engine Components for Model-Based Control (Second Report): Prediction of Combustion with High Speed Calculation Diesel Combustion Model". 2011. SAE Technical Paper 2011-01-2044.

[65] A. Yates and C. Viljoen. "An improved empirical model for describing auto-ignition". 2008. SAE Technical Paper 2008-01-1629.

[66] J. Hernandez, J. Sanz-Argent, J. Carot, and J. Jabaloyes. "Ignition delay time correlations for a diesel fuel with application to engine combustion modelling". *International Journal of Engine Research*, 11(3):199–206, 2010.

[67] M. Hillion, H. Buhlbuck, J. Chauvin, and N. Petit. "Combustion control of diesel engines using injection timing". 2009. SAE Technical Paper 2009-01-0367.

[68] F. Lafossas, M. Marbaix, and P. Menegazzi. "Development and application of a 0D DI Diesel combustion model for emissions prediction". 2007. SAE Technical Paper 2007-01-1841.

[69] I. Arsie, F. Di Genova, A. Mogavero, C. Pianese, G. Rizzo, A. Caraceni, P. Cioffi, and G. Flauti. "Multi-zone predictive modeling of common rail multi-injection diesel engines". 2006. SAE Technical Paper 2006-01-1384.

[70] S. Singh, L. Liang, S. Kong, and R. Reitz. "Development of a flame propagation model for dual-fuel partially premixed compression ignition engines". *International journal of Engine research*, 7(1):65–75, 2006.

[71] J. Livengood and P. Wu. "Correlation of autoignition phenomena in internal combustion engines and rapid compression machines". In *Symposium (International) on combustion*, volume 5, pages 347–356. Elsevier, 1955.

[72] M. Shahbakhti and C. Koch. "Dynamic modeling of HCCI combustion timing in transient fueling operation". *SAE International Journal of Engines*, 2(2009-01-1136):1098–1113, 2009.

[73] K. Sadabadi, M. Shahbakhti, A. Bharath, and R. Reitz. "Modeling of combustion phasing of a reactivity-controlled compression ignition engine for control applications". *International Journal of Engine Research*, 17(4):421–435, 2016.

[74] J. Bengtsson, P. Strandh, R. Johansson, P. Tunestål, and B. Johansson. "Hybrid modelling of homogeneous charge compression ignition (HCCI) engine dynamics-a survey". *International Journal of Control*, 80(11):1814–1847, 2007.

[75] N. Cavina, C. Siviero, and R. Suglia. "Residual gas fraction estimation: Application to a GDI engine with variable valve timing and EGR". 2004. SAE Technical Paper 2004-01-2943.

[76] J. B. Heywood. *"Internal combustion engine fundamentals",Chapter-5.* Mcgraw-hill New York, 1988.

[77] D. Rausen, A. Stefanopoulou, J. Kang, J. Eng, and T. Kuo. "A mean-value model for control of homogeneous charge compression ignition (HCCI) engines". *Journal of Dynamic Systems, Measurement, and Control*, 127(3):355–362, 2005.

[78] C. Aquino. "Transient A/F Control Characteristics of the 5 Liter Central Fuel Injection Engine". SAE Technical Paper 810494, 1981.

[79] E. Hendricks, O. Jannerup, and P. Sørensen. *"Linear systems control: deterministic and stochastic methods", Chapter-5.* Springer Science & Business Media, 2008.

[80] A. Mohammadbagheri, N. Zaeri, and M. Yaghoobi. "Comparison performance between PID and LQR controllers for 4-leg voltage-source inverters". *International Conference Circuit, System and Simulation*, 2011. Singapore.

[81] B. Anderson and J. Moore. *"Optimal control: linear quadratic methods", Chapter-3.* Courier Corporation, 2007.

[82] S. Mohan M, N. Naik, R. Gemson, and M. Ananthasayanam. "Introduction to

the Kalman filter and tuning its statistics for near optimal estimates and Cramer Rao bound". *Technical Report (Dept. of Electrical Engineering, IIT Kanpur, India) arXiv:1503.04313*, 2015. Accessed on 07-27-2017.

[83] MathWorks. "Kalman Filtering". `https://in.mathworks.com/help/control/ug/kalman-filtering.html`, 2017. Accessed on 07-03-2017.

[84] L. Wang. *"Model predictive control system design and implementation using MATLAB®", Chapter-2.* Springer Science & Business Media, 2009.

[85] M. Shahbakhti, M. Ghafuri, A. Aslani, A. Sahraeian, S. Jazayeri, and S. Azadi. "A method to determine fuel transport dynamics model parameters in port fuel injected gasoline engines during cold start and warm-up conditions". *Journal of Engineering for Gas Turbines and Power*, 132(7):074504, 2010.

Appendix A

Experimental Data for Model Parameterization

A.1   Data used for Parameterizing the Mean Value Models

Table A.1

Data used for Parameterizing the MVMs, RPM=1000, $T_{in} = 60^oC$

Exp #	SOC (CAD)	CA50 (CAD)	PR (-)	SOI (CAD bTDC)	m_{fuel} ($\frac{mg}{cyc}$)	MAP (kPa)	λ (-)	IMEP (kPa)	T_{exh} (^oC)	COV_{IMEP}[1] (%)	η_{ith} (%)
6	-6	8	10	35	21	96.5	1.35	535	493	5.2	23.83
8	-6	10	10	35	25	96.5	1.09	611	551	5.1	22.86
10	-6	6	10	40	22	96.5	1.28	563	497	5.1	23.94
12	-7	7	10	40	25	96.5	1.10	653	553	4.7	24.43
14	-7	4	10	45	23	96.5	1.26	680	522	4.8	27.66
16	-8	2	10	50	22	96.5	1.32	613	493	4.0	26.06
18	-9	3	10	50	24	96.5	1.17	607	532	4.4	23.66
23	-5	11	20	35	21	96.5	1.39	551	501	5.4	24.56
25	-5	12	20	35	25	96.5	1.10	727	572	4.3	27.22
27	-6	9	20	40	23	96.5	1.24	618	522	5.4	25.15
29	-7	8	20	45	23	96.5	1.22	694	530	5.6	28.24
31	-8	8	20	45	26.5	96.5	1.07	689	559	5.2	24.33
33	-5	13	30	35	22	96.5	1.36	549	522	7.2	23.37
37	-6	10	30	40	23	96.5	1.29	627	515	5.5	25.53
39	-7	8	30	45	22	96.5	1.32	634	511	3.6	26.98
41	-7	10	30	45	25	96.5	1.17	768	553	5.3	28.77
43	-8	6	30	50	25	96.5	1.17	664	539	3.8	24.87
49	-7	10	40	45	24	96.5	1.20	698	544	3.9	27.25
51	-7	12	40	45	27	96.5	1.06	716	579	4.1	24.84
53	-8	9	40	50	25	96.5	1.18	719	541	2.9	26.94
55	-8	9	40	55	23	96.5	1.31	699	507	3.7	28.47
15	-9	5	10	45	25	96.5	1.10	690	553	4.8	25.82
17	-11	2	10	50	23	96.5	1.23	611	520	4.4	24.85

Exp #	SOC (CAD)	CA50 (CAD)	PR (-)	SOI (CAD bTDC)	m_{fuel} ($\frac{mg}{cyc}$)	MAP (kPa)	λ (-)	IMEP (kPa)	T_{exh} (^oC)	COV_{IMEP} (%)	η_{ith} (%)
47	-6	15	40	40	27	97.5	1.08	589	595	4.5	20.44

---

[1]Measured using data recorded by FPGA

107

A.2 Data used for Validating the Mean Value Models

Table A.2

Data used for Validating the MVMs, RPM=1000, $T_{in} = 60°C$

Exp #	SOC (CAD)	CA50 (CAD)	PR (-)	SOI (CAD bTDC)	m_{fuel} ($\frac{mg}{cyc}$)	MAP (kPa)	λ (-)	IMEP (kPa)	T_{exh} (°C)	COV_{IMEP}^2 (%)	η_{ith} (%)
1	-4	15	10	30	19	96.5	1.53	516	474	5.2	25.40
3	-4	15	10	30	23	96.5	1.20	608	541	5.2	24.73
7	-6	9	10	35	23	96.5	1.21	560	510	5.3	22.78
9	-6	6	10	40	21	96.5	1.38	553	487	5.6	24.63
11	-6	6	10	40	23	96.5	1.23	575	517	4.2	23.39
13	-7	3	10	45	21	96.5	1.38	554	494	5.1	24.68
24	-5	12	20	35	23	96.5	1.22	597	535	4.8	24.29
26	-6	8	20	40	21	96.5	1.34	592	513	4.7	26.38
28	-6	9	20	40	25	96.5	1.10	662	560	4.8	24.78
30	-7	9	20	45	25	96.5	1.16	684	553	5.0	25.61
32	-8	5	20	50	23	96.5	1.28	611	514	4.4	24.86
35	-5	13	30	35	25	96.5	1.15	630	562	4.7	23.60
38	-6	11	30	40	25	96.5	1.15	742	556	4.8	27.79
40	-7	9	30	45	23	96.5	1.26	697	527	4.5	28.38
42	-7	6	30	50	23	96.5	1.31	621	512	5.0	25.28
44	-8	6	30	50	26	96.5	1.11	709	549	3.6	25.53
46	-6	15	40	40	25	96.5	1.17	712	565	4.9	26.68
48	-7	10	40	45	23	96.5	1.28	688	530	5.2	28.02
50	-7	11	40	45	25	96.5	1.17	700	553	4.3	26.23
52	-8	8	40	50	24	96.5	1.23	689	531	4.0	26.90
54	-7	10	40	50	27	96.5	1.08	805	567	3.3	27.93
56	-8	11	40	55	22	96.5	1.37	667	492	3.8	28.40
57	-8	10	40	55	25	96.5	1.18	732	529	4.1	27.43

Table A.2

Data used for Validating the MVMs, RPM=1000, $T_{in} = 60°C$

| Exp #	SOC (CAD)	CA50 (CAD)	PR (-)	SOI (CAD bTDC)	m_{fuel} $(\frac{mg}{cyc})$	MAP (kPa)	λ (-)	IMEP (kPa)	T_{exh} $(°C)$	COV_{IMEP}^2 (%)	η_{ith} (%)

---

[2] Measured using data recorded by FPGA

Appendix B

Injector Calibration

B.1   DI rail calibration

Figure B.1 shows the calibration of DI rail. The engine was run at 1000 rpm and fuel

was injected at an injection pressure of 100 bar for injection durations varying from

1ms to 5ms. The fuel consumption data for 100 cycles was recorded and averaged out

to calculate the fuel consumed per cycle. The data was plotted against the injection

duration and a linear fit was conducted to get the gain and offset values.
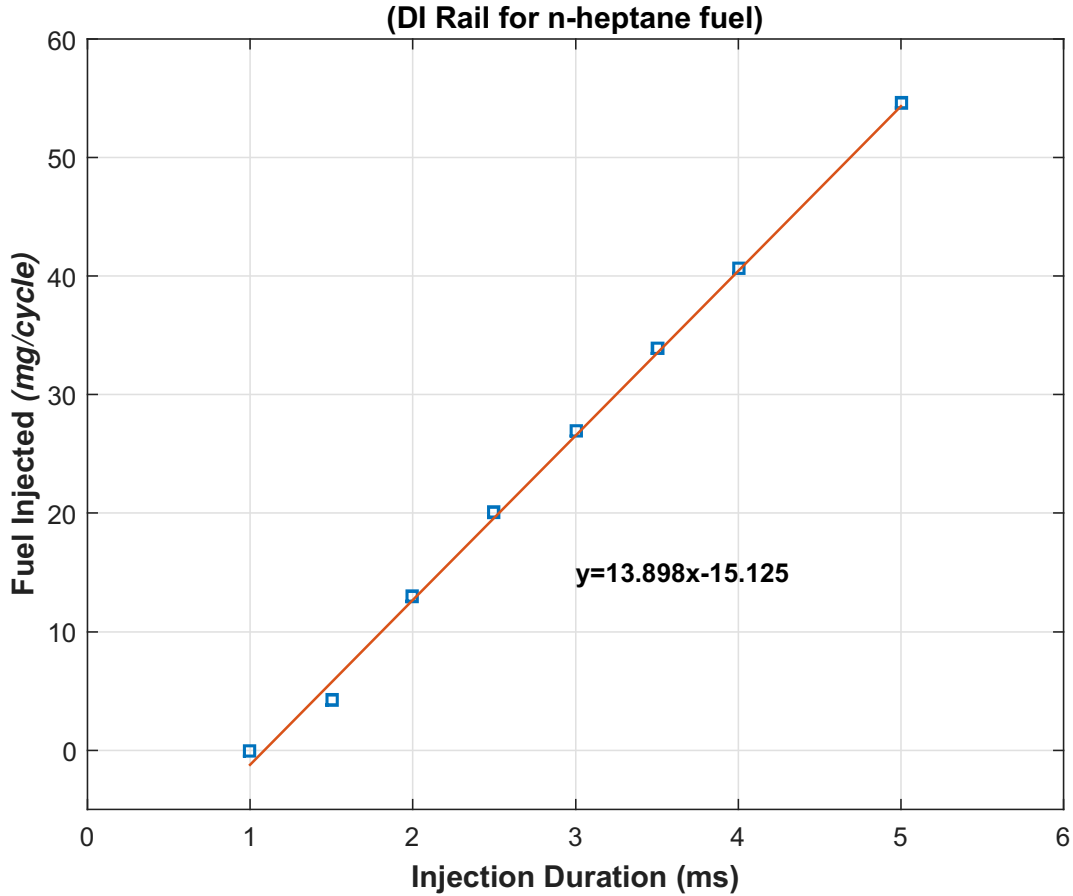
Figure B.1: Calibration of DI rail

B.2 PFI rail calibration

Figure B.2 shows the calibration of PFI rail running iso-octane fuel to the intake manifold. The engine was run at 1000 rpm and fuel was injected at an injection pressure of 3 bar for injection durations varying from 1ms to 10 ms. The fuel consumption data for 100 cycles was recorded and averaged out to calculate the fuel consumed per cycle. The data was plotted against the injection duration and a linear fit was conducted to get the gain and offset values.
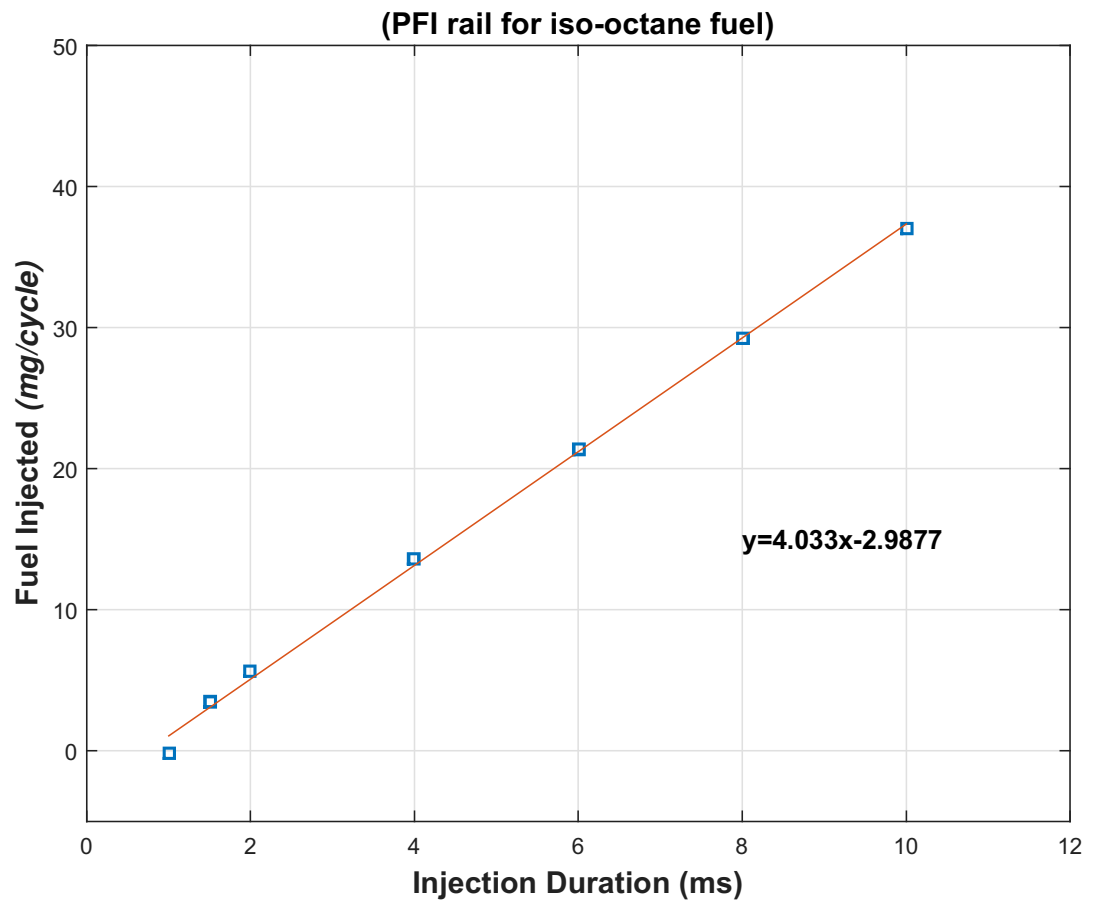
Figure B.2: Calibration of PFI rail

Appendix C

Calibration sheet for DI fuel injector

CALIBRATION CERTIFICATE

Model: 115A04
Serial #: 403
Description: Pressure Sensor
Type: Charge

Date: 6/7/2016
By: Roman Cichocki, Cal. Tech.
Station: Deadweight #6 (Test Procedure AT601-2)

Sensitivity*: 1.422 pC/PSI
206.2 pC/MPa
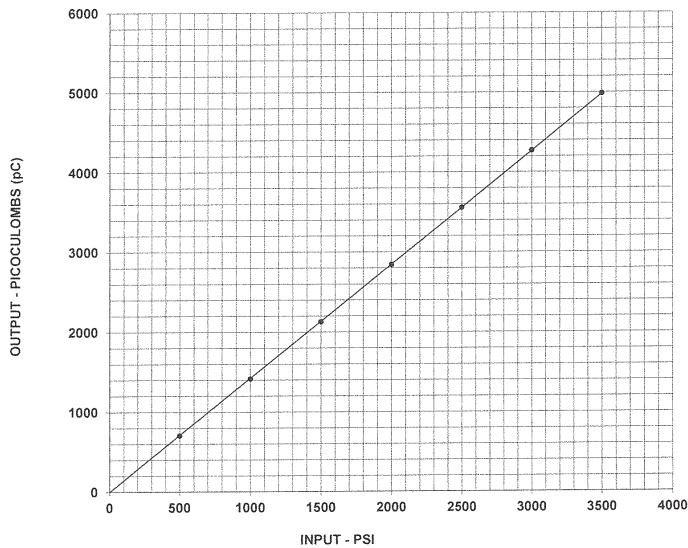
Temp: 70 deg F [21deg C]
Humidity: 42 %

Linearity*: 0.17% FS
Uncertainty**: +/- 1 %

Cert #: 612630

* Zero based, least-squares straight line.
** Measurement uncertainty represented using a coverage factor of k=2 which provides a level of confidence of approximately 95 %.

Condition of Unit:
As Found: Not applicable
As Left: In tolerance, new unit

TEST DATA

INPUT (PSI)	OUTPUT (pC)
500	703
1000	1414
1500	2128
2000	2841
2500	3555
3000	4269
3500	4982

Notes:
1 STATION #83
2 392 Deg F / 200 Deg C
3 Calibration is traceable to NIST and is accredited to ISO 17025 and ANSI/NCSL Z540.3.
4 NIST traceability through PCB control # CA1169.
5 This certificate may not be reproduced, except in full, without written approval from PCB Piezotronics, Inc.

ACCREDITED
CALIBRATION CERT #1862.01

PCB PIEZOTRONICS

Tel: 716-684-0001 Fax: 716-684-0987 Email: sales@pcb.com
3425 Walden Avenue, Depew NY 14043

ISO 9001 CERTIFIED

Page 1 of 1

Figure C.1: Calibration certificate of piezoelectric pressure transducer

Appendix D

Summary of Program and Data Files

D.1   Chapter 1

<div align="center">

Table D.1
Figure Files

File name	File Description
LTC_comparison_new.png	Figure1.2
Lit_review_RCCI.eps	Figure1.3
CLCC_RCCI_litreview.eps	Figure1.4
Thesis_Organization.eps	Figure1.5

</div>

Table D.2
Visio Files

File name	File Description
Lit_review_RCCI.vsd	Figure1.3
CLCC_RCCI_litreview.vsd	Figure1.4
Thesis_Organization.vsd	Figure1.5

D.2 Chapter 2

Table D.3
Figure Files

File name	File Description
LTC_Engine_Setup.eps	Figure2.1
ECU_setup.eps	Figure2.2

Table D.4
Visio Files

File name	File Description
LTC Engine Setup.vsdx	Figure2.1
ECU_Setup.vsdx	Figure2.2

D.3 Chapter 3

Table D.5
Figure Files

File name	File Description
Autoignition_litreview_MVM.eps	Figure3.1
SOC_pred.fig	Figure3.2
SOC_val.fig	Figure3.3
CA50_pred.fig	Figure3.4
CA50_val.fig	Figure3.5
DynamicModelSchematic.eps	Figure3.6
IMEP_val.fig	Figure3.7
Fuel_dyn_PR0.eps	Figure3.8
Fuel_dyn_PR20.fig	Figure3.9
Fuel_dyn_PR40.fig	Figure3.10
DynModel_VAl_PR.fig	Figure3.11
DynModel_VAl_SOI.fig	Figure3.12
DynModel_VAl_FQ.fig	Figure3.13

Table D.6
Visio Files

File name	File Description
Autoignition lit review_MVM.vsd	Figure3.1
DynamicModelSchematic.vsd	Figure3.6

File name	File Description
MVM_val_plots.m	M-file for plotting estimation and validation Figures 3.2 3.3 3.4 3.5 3.7 of MVM.
Model_pred_val_FPGA.m	M-file for estimation and validation of MKIM and CA50 models using steady-state data. The file uses the experimental data from RCCI_T60_param.xls file.
RCCI_dyn_60.m	M-file containing the detailed physical model
Dynamic_model.slx	Simulink file used for validating the dynamic model. Requires RCCI_dyn_60.m to run.
dyn_plots.m	M-file used to plot transient validation Figures 3.11 3.12 3.13 for the dynamic model.
Fuel_comp.m	M-file containing script used for estimating fuel transport model parameters and for plotting Figures 3.8 3.9 3.10
Data_analysis_akshat.m	m-code for saving raw data into .mat file
RCCI_T60_data_new.xlsx	Excel file containing data

Table D.8
Matlab Workspace Files

File name	File Description
FPGA_param_T60_data.mat	Matlab workspace file containing data points used for parameterization and validation of MVMs
FQ_TR.mat	File containing experimental data point used for validating dynamic model for varying FQ
PR_TR.mat	File containing experimental data point used for validating dynamic model for varying PR
SOI_TR.mat	File containing experimental data point used for validating dynamic model for varying SOI

D.4   Chapter 4

Table D.9
Figure Files

File name	File Description
nlfit.fig	Figure4.1
nonlin_val.fig	Figure4.2
Control_Model_Schematic.eps	Figure4.3
observer_val.fig	Figure4.4
LQI_sim.fig	Figure4.5
LQI_tracking.fig	Figure4.6
dist_rej_sim.fig	Figure4.7
dist_rej_exp.fig	Figure4.8

Table D.10
Visio Files

File name	File Description
Control Model Schematic.vsdx	Figure4.3

Table D.11
Matlab/Simulink Files

File name	File Description
LinearizationTest.slx	Simulink file to covert simplified model into state space form. Requires RCCI_dyn_nonlin_SISO.m to run
RCCI_dyn_nonlin_SISO.m	M-file containing simplified dynamic model.
CA50_nonlin_val_plot.m	M-file used to develop simplified fit for CA50
LQI_implementation.m	Simulink file for simulating LQI controller. Requires RCCI_dyn_60 to run.

Table D.12
Matlab Workspace Files

File name	File Description
Control_Transient_527.mat	LQI experimental result data file
Control_Transient_542.mat	Disturbance rejection experimental result file

D.5 Chapter 5

Table D.13
Figure Files

File name	File Description
MPC_PR_val.fig	Figure5.1
PR_MPC_exp.fig	Figure5.2
MPC_SOI_val.fig	Figure5.3
SOI_MPC_exp.fig	Figure5.4
single_MPC_multi_PR.fig	Figure5.5
Switched_MPC_exp_plot.fig	Figure5.6
sens_map.eps	Figure5.7
MPC_Control_Struct.eps	Figure5.8
sens_based_MPC.fig	Figure5.9
Sens_based_exp.fig	Figure5.10

Table D.14
Visio Files

File name	File Description
MPC Control Model Schematic.vsdx	Figure5.8

Table D.15
Matlab/Simulink Files

File name	File Description
MPC_1_PR.slx	Simulink file for MPC control with PR and FQ as control variable.
MPC_1_SOI.slx	Simulink file for MPC control with SOI and FQ as control variable.
Switched_MIMO.slx	Simulink file for switched MPC control
Sensitivity_MPC.slx	Simulink file for sensitivity based MPC control.

Table D.16
Matlab Workspace Files

File name	File Description
Control_Transient_513.mat	Experimental result data file for Figure 5.4
Control_Transient_516.mat	Experimental result data file for Figure 5.10
Control_Transient_519.mat	Experimental result data file for Figure 5.6
Control_Transient_521.mat	Experimental result data file for Figure 5.2

126

D.6 dSpace Files

Table D.17
dSpace Files

File name	File Description
Allengine68.slx	Simulink file used for controller implementation on dSpace MABX
Allengine68.ppc	Compiled object file for execution on the DS1104
HCCI_SI_Switch.lay	Layout file for control desk experiment
allengine68.sdf	System description file
Allengine68.trc	Variable description file
PR_10.mat	Data file for toolbox MPC. Needs to be loaded into workspace while building model
PR_20.mat	Data file for toolbox MPC. Needs to be loaded into workspace while building model
PR_30.mat	Data file for toolbox MPC. Needs to be loaded into workspace while building model
PR_40.mat	Data file for toolbox MPC. Needs to be loaded into workspace while building model

Appendix E

Letter of Permission

Letter of permission for Figure 1.2

Figure E.1: Letter of Permission